MECHANOTRANSDUCTION IN LIVING BONE:
EFFECTS OF THE KEAP1-NRF2 PATHWAY

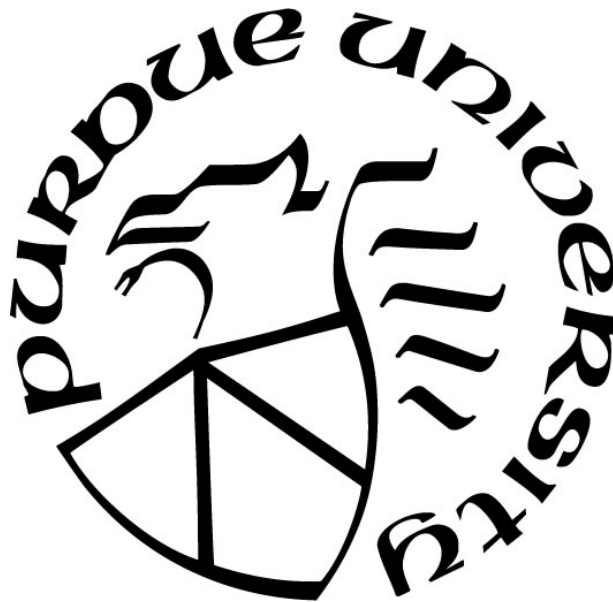by

Carlie Priddy

A Thesis

Submitted to the Faculty of Purdue University

In Partial Fulfillment of the Requirements for the degree of

Master of Science

Department of Biological Sciences

Indianapolis, Indiana

August 2019

THE PURDUE UNIVERSITY GRADUATE SCHOOL
STATEMENT OF COMMITTEE APPROVAL

Dr. Jiliang Li, Chair
    School of Science, Department of Biology

Dr. Guoli Dai
    School of Science, Department of Biology

Dr. Joseph M. Wallace
    School of Engineering and Technology

Approved by:
    Dr. James Marrs
        Head of the Graduate Program

For Richard and Kitty

ACKNOWLEDGMENTS

I have received a great deal of support throughout the course of my research, and the writing of this thesis. I would first like to extend the very greatest thanks to my advisor, Dr. Jiliang Li, for welcoming me into his lab and providing invaluable lessons and mentorship. I would like to thank Dr. Guoli Dai for serving on my graduate committee. I would also like to thank Dr. Joseph Wallace for serving on my graduate committee, and for access to and assistance with the biomechanical testing and analysis that made this project possible. For providing their expertise and training in countless histology techniques, I would like to thank Dr. Keith Condon and Drew Brown of the Histology Core of the IU School of Medicine. I would also like to thank all of the current and past members of the Li lab: Mustufa Shaikh, Caleb Russell, Chris Davis, Evelyn Shi, Eric Zhu, Devin Emery, Xiomara Regalado, Verayna Spell, Austin Pierce, Jennifer Alecio, and Jack Chen. Your support, friendship, and encouragement have meant the world to me.

TABLE OF CONTENTS

LIST OF FIGURES

ABSTRACT

Author: Priddy, Carlie. MS
Institution: Purdue University
Degree Received: August 2019
Title: Mechanotransduction in Living Bone: Effects of the Keap1-Nrf2 Pathway
Committee Chair: Jiliang Li

The Keap1-Nrf2 pathway regulates a wide range of cytoprotective genes, and has been found to serve a protective and beneficial role in many body systems. There is limited information available, however, about its role in bone homeostasis. While Nrf2 activation has been suggested as an effective method of increasing bone mass and quality, there have been conflicting reports which associate Keap1 deficiency with detrimental phenotypes. As Keap1 deletion is a common method of Nrf2 activation, further study should address the impacts of various methods of regulating Nrf2 expression. Also, little research has been conducted on the specific pathways by which Nrf2 activation improves bone quality. In this study, the effects of alterations to Nrf2 activation levels were explored in two specific and varied scenarios. In the first experiment, moderate Nrf2 activation was achieved via partial deletion of its sequestering protein, Keap1, in an aging mouse model. The hypothesis tested here is that moderate Nrf2 activation improves bone quality by affecting bone metabolism and response to mechanical loading. The results of this first experiment suggest a subtle, sex-specific effect of moderate Nrf2 activation in aging mice which improves specific indices of bone quality to varying degrees, but does not affect loading-induced bone formation. It is likely that the overwhelming phenotypic impacts associated with aging or the systemic effects of global Keap1 deficiency may increase the difficulty in parsing out significant effects that can be attributed solely to Nrf2 activation. In the second experiment, a cell-specific knockout of Nrf2 in the osteocytes was achieved using a Cre/Lox breeding system. The hypothesis tested here is that osteocyte-specific deletion of Nrf2 impairs bone quality by affecting bone metabolism and response to mechanical loading. The results of this experiment suggest an important role of Nrf2 in osteocyte function which improves certain indices of bone quality, which impacts male and female bones in different 7 ways, but did not significantly impact loading-induced bone formation. Further studies should modify the method of Nrf2 activation in an effort to refine the animal model, allowing the effects

of Nrf2 to be isolated from the potential systemic effects of Keap1 deletion. Future studies should also utilize other conditional knockout models to elucidate the effects of Nrf2 in other specific cell types.

INTRODUCTION

1.1 Bone Biology

The significance and complexities of bone should never be understated. It is the concerted effort of the 206 bones of the adult human skeleton which provide the weight-bearing framework for all other tissues [1-3]. Connective tissues attach muscle to bone, empowering the body with articulated movement [2, 3]. Protective bone structures such as the ribcage and skull shield vulnerable and vital organs. Bone marrow houses immune cells and the hematopoietic stem cells which continually replenish the blood cell supply [4]. Bone also serves as a responsive reservoir of calcium and phosphate, mediating the delicate balance of minerals in circulation [1, 3]. In these ways, bone tissue has supported the evolutionary journey of all vertebrates and is indispensable to their success [3].

In addition to its many roles in support of other body systems, bone tissue itself is more dynamic and communicative than is often recognized. Far from inert, living bone is in a constant state of mechanotransduction and remodeling [1, 3, 5-8]. It responds to strain [3]. It heals when damaged. It works throughout the life of an organism to maintain a delicate balance which maximizes the function and support provided [2, 3, 7, 9]. With ageing or disease, this balance can shift to favor resorption [7, 10]. Particularly in women, a loss of cortical – and even more significant loss of trabecular bone – is seen correlating to age [10]. This leads to dysfunction or disease of the bone tissue including osteoporosis, rheumatoid arthritis, and metastatic cancers [7].

In the case of osteoporosis, the strength and structural integrity of the bone is diminished through a loss of bone mass, leading to increased bone fragility [1]. To the 70 million people with this condition, a simple bone fracture can be life-threatening [7]. The musculoskeletal conditions resulting from injury, dysfunction, and ageing of bone tissue are the most commonly reported chronic medical conditions in adults in the United States. The medical costs associated with osteoporotic fractures is projected to reach $25.3 billion in the USA by the year 2025 [11]. While hip fractures represent the most common life-threatening fracture in osteoporosis patients, even minor fractures (such as vertebral, rib, or wrist fractures) have been linked to increased mortality rates [12, 13]. This type of injury is often followed by extended periods of decreased physical

activity, chronic pain, decreased muscle mass, and reduced quality of life [13]. This can initiate a steep decline in health which drastically increases the risk of death in following years [13]. Although the economic and social impacts of bone disease are immense, the precise underlying mechanisms of osteoporosis development have not been fully understood [1]. The microarchitecture and composition of subchondral bone has also been linked to osteoarthritis, a leading cause of disability [14]. Furthering the understanding of the specific molecular mechanisms which dictate the delicate homeostasis of bone strength is essential to finding specific and effective therapeutic targets for treatment and prevention of bone disorders [1].

1.2   Bone Tissue Structure

The unique composition and qualities of bone tissue set it apart from most other tissues, and unraveling its complexities has been the goal of investigators for over 300 years [1, 15]. It is comprised of an organic phase embedded with mineral crystals [5]. The balance of these components determines the strength and mechanical properties of bone [2]. Immature bone is flexible and collagenous, slowly mineralizing over the course of development into mature bone [16]. Mature bone exists in a fluctuating state, maintaining a delicate balance of stiffness (as bone must provide weight-bearing strength) and flexibility (as excessive rigidity or brittleness of bone results in damage upon weight bearing) [2, 3]. Mature bone tissue is generally divided into two forms: the cortical (or compact) bone and the trabecular (also known as cancellous) bone, which possess unique microarchitecture [5]. In order to address the network of intricacies which allow the vast functions of bone to be carried out continuously, it is best to understand the composition and structure on a hierarchical scale [15].

1.2.1   Bone Composition

Bone tissue is a matrix of biopolymers, mineralized to varying degrees with calcium hydroxyapatite crystals ($Ca_{10}(PO_4)_6(OH)_2$) [2, 4, 5, 17]. The organic phase of bone is primarily type I collagen, but also includes other noncallagenous proteins (NCPs) associated with the matrix, like osteocalcin, osteonectin, osteopontin, proteogloycans and glycoproteins [4, 9]. Only around 15% of these NCPs are located within bone cells, and the rest occupy the extracellular matrix [9]. While they make up only a small fraction of the matrix, these noncollagenous proteins serve important functions [17]. Several glycoproteins take part in mineralization of

newly-formed bone, proteoglycans support cartilage and skeletal development, soteocalcin regulates mineral homeostasis, and osteonectin promotes formation and mineralization of new bone tissue [9]

The impressive tensile strength and flexibility of bone is owed to the triple helix conformation of its large proportion of collagen, reinforced with cross-links that maintain structure while absorbing mechanical loads [2, 5]. While human bone, on average, is about 60 percent mineralized; the degree of bone mineralization varies with function, from stiff high fidelity structures like the auditory ossicles (around 90 percent mineralized) to shock-absorbing and relatively flexible structures like antlers (only around 40 percent mineralized) [2]. All bone shares the fundamental building block of the mineralized collagen fibril, and variations in the structure and composition of bone on a micro and macro scale determine its function and as a whole [15, 16]. The level of strength and resistance to fracture determined by the vast composite of variables within bone is referred to as bone quality, and is determined by a combination of structural qualities including: bone turnover rate, bone architecture, intrinsic properties, and accumulated microdamage [9].

1.2.2   Bone Microstructure

The most fundamental building block of bone is a single mineralized collagen fibril [15]. On a microstructural level, bone can be categorized by the method of depositing these fibers [9]. In lamellar bone, they are slowly and neatly arranged into discrete visible sheets [9]. On the other end of this spectrum, woven bone is a haphazard arrangement of rapidly mineralized and disorganized fibers [9]. Bone that is newly formed where no previous bone existed is referred to as primary bone, while bone that is deposited where bone has previously been resorbed is called secondary bone.

Primary bone microarchitecture is also separated based on morphology into three categories: primary lamellar bone, a strong and dense series of laminar sheets with minimal vasculature located on bone surfaces; plexiform bone (also referred to as fibrolamellar bone), a quick-forming composite of lamellar and nonlamellar bone woven with a network of vasculature; and primary osteons, which form by filling in a vascular channel within an established bone with concentric layers of new bone [9]. Secondary bone forms after the resorption of original bone

tissue and develops a network of canals now known as haversian systems, first described in the late seventeenth century in some of the earliest utilizations of the light microscope [18, 19]. The tunnels formed by resorption are known as lacunae, while the new bone which fills them is referred to as a secondary osteon, first characterized by Gebhardt in more accurate detail after the emergence of the polarizing microscope in the nineteenth century [15]. These haversian systems generate porosity in the bone, and the patterning of these microstructures determines the strength, rigidity, and mass of the bones, all of which heavily factor into the mobility and fitness of an organism [7, 9].

Damage can also be seen and influenced at the microscopic level of bone tissues. Microdamage occurs as a result of the repetitive load bearing normally carried out by bone [9]. This damage first presents as microcracks – but if it accumulates faster than can be repaired by the bone reformation system, fractures become more likely [9]. As a microcrack progresses through solid bone, it has trouble penetrating the cement line of an osteon (due to the tightly packed concentric layers of bone oriented at a different angle than the surrounding bone) [2]. In this way, the osteon structure plays a direct role in resisting detrimental effects of microdamage.

1.2.3   Bone Macrostructure

On a macroscopic scale, mature bone is divided into two categories: cortical (or compact) bone, and cancellous (also referred to as trabecular or spongy) bone [4, 9]. Cortical bone is the strong, protective, largely solid (only around 3-5% porous) bone material which makes up the diaphyses and skull [2, 9]. Cortical bone provides rigid strength which allows for mobility and impressive weight-bearing ability, but is susceptible to fracture [2]. Cancellous bone, first described by Monro [16], is formed from interconnected plates and rods of bone with lamella oriented roughly parallel to the trabecular surface [9]. Cancellous bone is primarily found in the ribs, vertebrae, and metaphyses of the long bones [9].

The complete bone structure is formed by a combination of cancellous and cortical bone surrounding the bone marrow [4]. The outer surface of the cortical bone is referred to as the periosteal surface, and the inner surface which faces the marrow cavity if referred to as the endosteal or endocortical surface [2]. Bone formation on the periosteal surface increases the bone width, while increases in bone length are achieved through endosteal bone formation [2].

Combined with mineral composition, the micro- and macro-structural properties define the strength and quality of a bone. The organization, size, and number of trabeculae within cancellous bone are impactful factors in bone quality. This is where the most impactful effects of aging are seen in the bone, as trabecular density decreases significantly with age [10].

1.3   Bone Cells

1.3.1   Osteoclasts

Osteoclasts are large, multinucleated bone cells with the highly specialized function of bone resorption [1, 3, 9]. Being exclusively responsible for resorption, osteoclasts are a key factor in bone homeostasis (both modeling and remodeling) [4, 9]. Osteoclastogenesis is the process by which mature osteoclasts are derived from hematopoietic stem cells (HSCs) in the bone marrow [1, 3, 4]. After the HSCs become multipotent progenitors, a subset will further differentiate into common myeloid progenitors (CMPs) – and it is these CMPs that give rise to the monocyte/macrophage lineage cells which include osteoclast precursors [3, 9]. Certain environmental factors – such as calcium gradients, interleukin-3 (IL-3), granulocyte-macrophage colony-stimulating factor (GM-CSF), and macrophage colony-stimulating factor (M-CSF) – induce these monocyte/macrophage lineage cells to be recruited towards the bone service, proliferate, and become differentiated through a series of steps into committed osteoclast precursors [9]. Committed osteoclast precursors are RANK+ and can be activated by receptor activator of nuclear factor K-B ligand (RANKL), a member of the tumor necrosis factor receptor family of ligands [1, 3, 9].

The activation of RANK by its ligand initiates a signaling cascade involving many cytoplasmic factors and downstream signaling pathways, including: TNF receptor-associated factor 6 (TRAF6), TNF1, c-Fos, NF-KB, IL-1, PGE2, TGFi, inhibitor of NF-ÙB kinase (IKK), c-Jun N-terminal kinase (JNK), p38, extracellular signal-regulated kinase (ERK) and Src pathways [3, 7, 20]. RANKL has been identified as the most important factor in this highly-involved process of differentiation culminating in expression of the master transcription factor of osteoclastogenesis, NFATC1, which induces the fusion of osteoclast precursors and structural changes associated with the formation of mature osteoclasts (the completion of osteoclastogenesis) [3, 7, 20].

Several unique and dramatic morphological changes occur during osteoclastogenesis [21]. A number of precursor cells fuse through a remodeling of the phospholipids within their cell membranes [3]. Any of these cells containing 3 or more nuclei are considered mature osteoclasts [9]. While most contain 3-20 nuclei, it is common to see even more in a single cell (although there appears to be an ideal size for resorption within the average range, as the largest osteoclasts have been shown to have reduced bone resorbing activity) [9]. The large size of these cells allows them to cover and resorb a wide area of the bone surface quickly and efficiently [3]. The actin cytoskeleton also rearranges, generating a polarization within the cell that results in the formation of opposing apical and basolateral functional domains [7, 9]. This polarization is a key step which allows the osteoclast to attach to and migrate along the bone surface while resorbing bone [9]. At the interface of the apical domain and bone surface, the osteoclast forms a firm attachment to the bone surface known as the sealed compartment (or sealing zone), within which bone resorption occurs [4, 7, 9].

The sealed compartment surrounds another structure, a convoluted membrane of transport vesicles fused to the apical membrane that is known as the ruffled border [9]. The area between these two borders allows for the exchange of materials between the osteoclast and the sealing zone [9]. Protons generated by carbonic anhydrase and hydrolytic enzymes including cathepsin K (CtsK) and matrix metalloproteinases (MMPs) are pumped across the ruffled border to acidify this extracellular compartment and degrade the bone matrix [3, 4, 22]. Chloride ions are pumped back across the border as a counterbalance to the proton secretion [9]. This acidification dissolves the inorganic components of the bone matrix, while the enzymes degrade the organic components [3, 4]. The products of resorption are then internalized from the sealing zone into the osteoclast and may be transported to lysosomes for degradation or released through the basolateral surface into circulation [7, 9]. This process results in the successful degradation and resorption of the underlying bone, leaving behind a cavity in the bone surface [5]. Upon completion of resorption, osteoclasts are known to undergo apoptosis, although the exact mechanisms underlying this process are not completely understood [9].

While degrading the bone matrix may sound detrimental, it is actually a vital step in healthy bone homeostasis. Bone resorption during development allows for the shaping of growing bones and excavation of the marrow cavity [2]. In adults, osteoclasts are recruited to sites of damage,

where they excavate damaged bone tissue while simultaneously releasing growth factors (like TGF-β) that initiate the migration of osteoblasts which refill the cavity with new bone matrix [1, 2]. The key to healthy bone homeostasis is balance within these systems [2]. The importance of maintaining an appropriate level of RANK/RANKL activity has been demonstrated by several studies – while the presence of RANK is absolutely necessary for normal bone homeostasis, its constitutive activation has been linked to several bone diseases [3]. Skewing the balance in favor of osteoclast activity reduces bone mass and increases bone fragility, while downregulating osteoclast activity results in increased bone mass and a reduced damage repair mechanism through reformation – with a drastic shift in either direction being linked to various bone diseases [2, 3, 9]. This makes the osteoclast an excellent target for the treatment of diseases linked to excessive bone resorption [20].

Of all the factors involved in the recruitment of osteoclasts, studies have shown that two, M-CSF and RANKL, are necessary and sufficient to induce osteoclastogenesis [3, 9, 21]. There are two commonly used models for studying osteoclastogenesis, the bone marrow macrophages (BMMs) and RAW 264.7 cells. These two cell types have the ability to differentiate into osteoclasts for use as study models, but a study by Ng et al found that RAW 264.7 cells undergo osteoclastogenesis even in the absence of M-SCF, suggesting that these cells may not be the ideal model of the in vivo osteoclast (which is M-CSF-dependent) especially when studying any downstream functions associated to M-CSF [21].

1.3.2 Osteoblasts

While bone matrix is dissolved and resorbed by the osteoclasts, new bone tissue is deposited by another cell type – the osteoblast [1, 5]. Osteoblasts are mesenchymal cells derived from precursors of neural crest or mesodermal origin [8]. Once recruited, active osteoblasts localize on the bone surface and secrete osteoid, a material composed type I collagen and other bone matrix proteins [4, 23]. They also mediate the mineralization of this newly formed osteoid through the secretion of matrix vesicles and alkaline phosphatase [1, 4]. Osteoblasts possess receptors for several hormones, including estrogen, vitamin D, parathyroid hormone (PTH) and parathyroid-related protein (PTHrP) [1]. As the main producer of RANKL, osteoblasts direct osteoclast recruitment and work in coordination with osteoclasts to carry out bone reformation [1, 8].

The osteoblast lineage refers to any cell that has ever committed to osteoblast differentiation; from committed precursor cells with the potential to become osteoblasts, to currently active bone-forming osteoblasts, to lining cells which no longer produce osteoid but appear to guard the bone surface, to osteocytes which were once active osteoblasts before becoming embedded in the osteoid or mineralized matrix [23]. Recruitment of precursor cells to proliferate near the bone surface is mediated by the cytokines insulin-like growth factor-I (IGF-I) and transforming growth factor beta (TGF-β) [4]. Contingent upon the activity of bone transcription factor Runt-related transcription factor 2 (Runx2), they also express matrix metalloproteinase-14 (MMP-13) in response to TGF-β1[22]. The precise molecular pathway to the differentiation into mature osteoclasts has not been comprehensively defined, but has been shown to involve the cytokines bone morphogenetic protein (BMP) and Wnt (a portmanteau of the previously-given names Wingless and Int-1), and to be dependent on the presence of the transcription factors Runx2 and Osterix (Osx) [4, 8, 23]. Frizzled and sclerostin are known Wnt antagonists that have been shown to inhibit osteoblast differentiation [4].

Osteoblasts have been extensively researched, given that increases in their activity result in increased bone formation and a potential for therapeutic mediation of bone diseases [1, 23]. These cells can be readily identified in tissue sections as they associate closely with the bone matrix (and are easily distinguishable in size and nucleus number from osteoclasts), but are difficult to quantify from in vitro studies lacking osteoid structures [23].

1.3.3   Osteocytes

Occassionally, mature osteoblast cells become embedded in an unmineralized, fluid filled lacuna within the osteoid they produce [2, 4, 24]. These cells develop into a third type of bone cell – the osteocyte [2, 4]. This happens regularly enough that no point within any bone is more than a handful of micometers from a lacuna containing an osteocyte [2, 24]. The osteocyte has a unique structure, with dendrites that extend outwards through small channels called canaliculi that connect to other lacunae, creating a lattice throughout the bone [3, 24]. Focal adhesions anchor the osteocytes in place within the lacunae, and the dendrites conect with those of adjacent osteocytes at gap junctions [3, 24]. They are the longest lived, most numerous, and yet least researched of all bone cells [2].

The osteocyte is thought to be the mechanosensitive cell of bone tissue, and to coordinate the activities of osteoblasts and osteoclasts in response to mechanical strain [3, 4, 24]. The precise underlying mechanism by which osteocytes communicate strain and command the other bone cells has not been fully explained [3]. It is believed that they sense mechanical strain via fluid shear stress exerted on the cell membrane during mechanical loading of the bone [10, 24]. While this force effect would only occur at one instance upon continuous static loading, its magnitude would increase proportionately with the frequency of dynamic loading (which offers a probable explanation for reported findings that only dynamic loading results in increased bone formation) [24]. In response to mechanical stress, osteocytes communicate with other osteocytes through secreted paracrine signals or through calcium signals at the gap junctions between their dendrites [24]. They have been found to be responsive to signaling factors involved in bone formation, such as PTH, and to produce signaling factors which directly influence the activity of osteoblasts and osteoclasts [4, 24]. Osteocytes are the primary constitutive source sclerostin, an important indirect inhibitor of osteoblast activity [4, 24]. Mechanical loading reduces sclerostin expression, which in turn increases osteoblastic activity [24]. Osteocytes also produce RANKL which activates osteoblasts who in turn secrete RANK that stimulates osteoclast activation [1, 4]. In this way, the osteocyte is equipped to coordinate the activities of the whole basic multicellular unit (BMU) responsible for bone remodeling to shape and mold the bone structure overall in response to mechanical signals [4]. It is very likely that the death of an osteocyte is commounicated through changes in molecular signalling to effectively announce a site of significant damage within a bone, and this could be an underlying mechanism behind the quick targeted repair of bone fractures [2].

1.3.4   Other Cell Types

Several other cell types exist in close association with the three primary bone cell types. Chondrocytes are the cells responsible to the production and maintenance of cartilage, and are located around the bone extracellular matrix and within the bone marrow that also houses B cells, T cells, macrophages, hematopoietic cells, and stromal cells [4].

1.4 Bone Cell Communication

Because bones respond so specifically to stimuli, it is clear that there must be methods of communication driving the appropriate responses. Several avenues of potential molecular communication have been studied, describing the significance of paracrine signals in bone cell function [2, 23]. Bone tissue is also remarkably innervated, so neuropeptide signalling has been studied extensively and subsequently linked at least five distinct neuropeptides (calcitonin gene-related peptide, neuropeptide Y, substance P, vasoactive intestinal peptide, and tyrosine hydroxylase) to a shift in bone homeostasis which favors formation over resorption [25].

Although the act of remodeling bone, through the resorption of old bone and deposition of new osteoid, is carried out by the basic multicellular unit consisting of the osteoclast and osteoblast, this cannot be the true origin of this process [2]. In order to coordinate the activity of these cells in direct response to stimulus such as mechanical strain or damage acumulation, there must be participants which sense the stimulus and communicate instructions for the appropriate response of other participants [2]. This master coordinator is believed to be the osteocyte [2, 4]. These three cell types are likely in close communication facilitated by paracrine signaling and gap junctions, as evidenced by previous studies demonstrating the necessity of cell-cell contact in order for osteoblasts to function properly [23, 25]. The importance of gap junction intercellular communication (GJIC) for proper function of osteoblasts and osteocytes has been specifically demonstrated [25].

Other cell types, such as marrow stromal cells and T cells have been identified as members of the communicative network that drives bone remodeling, as have factors such as BMPs, TGF-β, and Smad family molecules [7, 25].

1.5 Bone Metabolism

Bone metabolism is the general term for the various complex alterations bone tissue undergoes throughout a lifetime [1]. It can be divided into the initial construction of bone, known as modeling; and the dynamic reconstruction of existing bone, known as remodeling [2, 26]. Both are cellular processes by which the size, shape, and architecture of the bone are changed [2, 26].

1.5.1 Bone Modeling

Bone modeling is the method of initial formation of new bone onto an existing bone surface where none had previously existed, which occurs during growth and development [2, 9]. The term also applies to osteoclastic resorption that is not coupled with osteoblast activity [9]. This is the method by which growing bones elongate and change shape, and is regulated by several interacting factors in the microenvironment [2, 4, 5, 9]. Since bone modeling always takes place on existing bone surface, the initial ossification of cartilagenous structures into embryonic bones is not considered modeling [9]. While the modeling process is principal to regular vertebrate development, its underlying molecular mechanisms are not fully known [27]. A few members of the expansive network of biomolecules and growth factors interacting in this process include: PTHrP, Runx2, Osx, MBP, and Hedgehog signaling [5, 25, 27].

1.5.2 Bone Remodeling

In contrast to bone modeling, remodeling is a change in existing bone resulting from the coupled activities of bone resorption and formation carried out by the basic multicellular unit (BMU) of osteoclast and osteoblast [1, 7, 9, 20]. A third type of cell with a poorly understood function, the lining cell, is laid along the sites of osteoclast excavation between resorption and formation (a phase referred to as the reversal phase). It is this tightly-coupled process that makes the precise replacement of resorbed bone with newly-formed bone possible, thereby removing old or damaged tissue continuously without sacrificing bone quality [5, 8]. This process maintains the integrity of the adult skeleton and is the primary source of any morphological changes that occur in the bones throughout the adult life of an organism [9]. Remodeling can also be utilized for the release of minerals into circulation in the case of a mineral deficiency [1].

The repeating cycles of osteoclastic resorption and paired osteoblastic formation maintain a balance which allows the skeleton to carry out its protective and locomotive functions throughout the lifetime of the organism [2, 3]. Any shifts in this balance can be detrimental to bone health; and some, such as those associated with ageing, appear inevitable in long-lived species [1, 2]. Rapid remodeling results in an increase in the proportion of immature bone tissue, which is more susceptible to fracture than more mineralized bone [2]. Because trabecular structures have significantly greater surface area proportional to mass, trabecular bone turns over

much faster than cortical bone [2]. A decrease in osteoblast activity, as is commonly seen with ageing, causes disequilibrium in the BMU that decreases overall bone mass [5].

Sophisticated signaling directs the process of bone remodeling, insuring not only that specific damaged or stressed sites receive focused attention; but that the osteoclasts are always recruited first, to clear the way before the osteoblasts refill the gaps [2, 9]. Signals released into the microenvironment from all three bone cell types are likely in communication during initiation [2]. The osteocyte directs the initiation of remodeling to sites of damage or strain, where osteoblasts and osteoclasts are recruited and form a feedback loop which promotes their activity [2]. The various factors involved include Wnts [8], TGF-β, MMP-13, Runx2 [22], and other hormones, cytokines, matrix proteins, and growth factors [8].

1.6   Skeletal Mechanotransduction

Mechanotransduction is the ability to detect mechanical signals and transduce them into physiological responses [10, 28-30]. The term can be strictly defined as the conversion of mechanical energy into chemical energy; and, within biological systems, this refers to the ability of living tissues to respond to sensed mechanical stimuli from the environment [30]. The study of mechanotransduction in bone originated with Julius Wolff, an anatomist and surgeon who first suggested that bone remodels in response to physical load bearing (this concept linking mechanotransduction with bone homeostasis became known as Wolff's Law) [30]. The understanding of bone mechanotransduction has been greatly increased thanks to advancements in molecular and cellular biology, allowing specific investigations into the signaling pathways involved in this process [30].

Many body tissues change or remodel in response to detection of mechanical strain. The previous decade of research has demonstrated that this potential exists in all cell types, and is not limited to cell types with well-known adaptations for sensory transduction (such as neurons or the hair cells of the ear) [10, 30]. It is apparent that the mechanisms behind mechanotransduction are complex, and several cellular components have been suggested as possible sites of mechanotransduction, including: cell-matrix adhesions, cell-cell adhesions, the cytoskeleton, cell membranes, and extracellular environment [10, 29, 30]. Intercellular and extracellular filaments form a woven network that serves as the basic unit of load bearing in all cell types [30].

Because bone serves a primary function of supportive load-bearing in the body, it is no surprise that mechanotransduction plays a significant role in bone homeostasis. Mechanical loading initiates a signaling process (referred to as activation) which allows the bone tissue to selectively remodel, increasing formation while simultaneously suppressing resorption [10, 24, 26]. This response is localized to the area of mechanical strain, and can be reversed if that area enters a prolonged state of disuse [24]. The results of this response can be clearly illustrated in human models when comparing the dominant and non-dominant arm bones of college baseball players, with the dominant arm bones containing over 60% more mass as a result of the selective and repetitive loading of that arm over time [24]. This response can be replicated using noninvasive loading to selectively apply mechanical strain to only one ulna of mice over a period of time [31]. It has been shown that dynamic, cyclical loading produces a significant bone formation response, but static/stationary continuous loading fails to reproduce the same response [24]. This increase in bone mass is an adaptive way for the body to reduce the strain that will be endured by any repeated loadings [10]. Increasing the frequency of dynamic loading has been shown to increase the bone formation response, up to a plateau of the trend at around 10 Hz [24].

Aging may have significant implications in mechanotransduction. In humans, it has been noted that bone formation in response to mechanical loading (through physical activity and exercise) is greatest in young individuals, and diminished in the elderly [10]. There is limited and conflicting information available about the role of aging in mechanotransduction [10]. It has been suggested that age may affect mechanotransduction through a reduction in cell sensitivity, a change in hormone or paracrine factor levels, or even simply via a decline in the number of viable mechanosensitive cells like osteocytes and MSCs [10].

The molecular signaling pathways involved in mechanotransduction of living bone are not fully known, but involve the release of ATP and calcium ions followed by the actions of messenger molecules like prostaglandins, nitric oxide, and protein kinases [24]. Within bone tissues, the osteocyte is believed to be the primary mechanosensitive cell type [3, 4, 24, 26]. Osteoblasts and osteoclasts are also likely involved in bone signal communication, as they each release nucleotides capable of functioning as autocrine and paracrine signaling factors in response to mechanical strain [32]. Potential mechanosensors within bone cells include: calcium channels (both stretch- and voltage-sensitive), adhesion proteins bound by integrins to the extracellular

matrix, and a G protein-coupled receptor (GPCR) [24]. Several osteogenic factors have been shown to mediate loading-induced bone formation, including prostaglandins, nitric oxide, TGF-β, and insulin-like growth factors [28, 32].

1.7   The Keap1-Nrf2 Interaction

1.7.1   Stress Response

Cellular stress has many origins and products. Natural processes can result in stress. Stress can also result from exogenous sources like drugs, pollutants, and food additives. These foreign substances are referred to as xenobiotics. Biological systems manage stress through the process of detoxification, which occurs in two phases. Phase I detoxification involves the breakdown of xenobiotics into electrophiles, metabolites that still have deleterious potential [33]. True detoxification occurs during phase II detoxification, where these intermediates are metabolized into non-toxic products [33].

Xenobiotics contribute to the redox reactions which produce reactive oxygen species (ROS) [34]. However, ROS also form as a natural byproduct of cellular function [35]. While elevated ROS levels result in oxidative stress and cell damage, it has been firmly established that ROS are required, at least in small amounts, to maintain normal cellular function [28, 35, 36]. The dilemma faced by all aerobic eukaryotes is that oxygen, while ubiquitous and vital, poses inherent threat (this is called the "oxygen paradox") [35]. This threat has been building for over 2 billion years, ever since the reservoir of organic matter on the planet became fully saturated with oxygen produced by the newly evolved photosynthetic cyanobacteria and excess oxygen accumulated – likely leading to the first mass extinction of anaerobic organisms unable to cope with the changing atmosphere [37]. Methods of maintaining the appropriate balance of ROS in biological systems include antioxidants and free radical scavengers. The Keap1-Nrf2 pathway is responsible for a key cytoprotective transcriptional cascade which combats oxidative stress of many sources including xenobiotics, ROS, radiation, and endogenous stressors [38-40].

1.7.2   Nrf2

Nuclear factor erythroid 2-related factor 2 (Nrf2), first characterized in 1994, is a transcription factor considered a master regulator of antioxidant cytoprotective genes [1, 41, 42]. It is a

member of the basic leucine zipper family of proteins – along with the ubiquitously expressed Nrf1, the placenta- and liver- specific Nrf3; and NF-EF, which is only expressed in erythrocytes [1]. Nrf2 is the primary mediator of redox stress in the basic leucine zipper family, and is ubiquitously expressed [1, 43]. Under unstressed conditions, Nrf2 is maintained in the cytoplasm, bound to its repressor Kelch-like ECH-associated protein 1 (Keap1) [43]. When activated, Nrf2 mediates a powerful signaling cascade necessary for phase II detoxification involving several antioxidant, cytoprotective, and detoxifying enzymes [33, 39]; which has been demonstrated in an abundance of disease models including cancer, diabetes, and liver disease [44, 45]. Nrf2 activity has been a highly popular topic of investigation for the past two decades [39], which has resulted in significant revelations of the molecular mechanisms behind its cytoprotective cascade [1].

Along with its basic leucine zipper domain, Nrf2 also contains an N-terminal hydrophobic domain, Cap'n'Collar (CNC) domain, transcriptional activation domain, and a Keap1-binding domain [1, 46]. The Keap1-binding domain maintains the association with the repressor Keap1 under basal conditions [43]. The leucine zipper domain allows heterodimerization with small Maf or Jun proteins and binds Nrf2 to an antioxidant response element (ARE) [1]. While the bulk of research has focused on the role of Nrf2 as a transcription factor, recent studies have also illustrated its importance as a protein whose presence is necessary for certain processes, such as angiogenesis [43].

High ROS levels pose a threat to many biological systems and contribute to a multitude of disease models including cancer, infertility, and neurodegenerative disease [28, 35]. They arise from the breakdown of molecular oxygen into atomic oxygen, which has a single unpaired electron – making it a free radical [35]. In response to increasing levels of stress molecules (electrophiles, ROS, or metabolites of phase I detoxification), Nrf2 is released from its sequestering protein, Keap1, and permitted to translocate into the nucleus [1, 40, 43]. There, Nrf2 binds to the antioxidant response element (ARE) and increases the expression of cytoprotective genes like heme oxygenase 1 (HMOX1), NADPH quinone dehydrogenase 10 (NQO1), and the glutamate-cysteine ligase modifier subunit (GCLM) [43]. Nrf2 activates enzymes necessary for phase II detoxification of ROS and electrophiles into non-toxic products [33].

1.7.3 Keap1

After Nrf2 became a hot topic of broad research, Kelch-like ECH-associated protein 1 (Keap1) was discovered during the in-depth analysis of Nrf2 regulation [33]. Its successful discovery was first described by Itoh, Mimura, and Yamamoto in 2010 [33]. Keap1 holds Nrf2 by associating with its N-terminal domain [1, 33]. Under low stress conditions, Keap1 prevents the translocation of Nrf2 to the nucleus and ushers it towards degradation via the ubiquitin-proteasome pathway mediated by Cul3/Rbx1 [1, 33]. Exposure to stress (detected as xenobiotics, ROS, or intermediate products of phase I detoxification) leads to the oxidation of the cysteine residues which maintain the attachment to Nrf2, leading to its release [1, 40, 43]. The free Nrf2 is then translocated to the nucleus for activation and initiation of phase II detoxification. In this way, Keap1 acts as a sensor of stress and regulates cellular detoxifying ability accordingly by regulating Nrf2 activation [1, 40, 43].

Keap1 is a homodimeric protein similar to the Drosophila protein Kelch [33, 40]. It contains two canonical protein interaction domains: bric-a-brac tramtrack broad complex (BTB) and Kelch (also known as the double glycine repeat or DGR), as well as two other domains: the intervening region (IVR) and C-terminal region (CTR) [40]. The BTB domain dimerizes Keap1, allowing ubiquitin conjugation to the lysine residues of the N-terminal domain of Nrf2; the DC domain (a collective term for the DGR and CTR) forms the physical interaction with the Nrf2 N-terminal domain, and the IVR promotes the ubiquitination of Nrf2 [40]

1.7.4 Significance of this Pathway

As a master regulator of cytoprotective and antioxidant function, the Nrf2 pathway is a very attractive potential therapeutic target [39, 40, 47]. Various endogenous, environmental, and pharmacological inducers have been shown to activate Nrf2 [48]. Some natural activators include the isothiocyanates of cruciferous vegetables, organosulfur found in garlic, isoflavanes found in beans and coffee, phenols from ginger, and polyphenols from tea. Synthetic activators are also available, such as: trivalent arsenicals, dithiolethiones, and oxidizable diphenols [39]. The level of interest in boosting Nrf2 activation in humans is understandable, since the Keap1-Nrf2 pathway mediates the oxidative stress response, innate immunity, and metabolic homeostasis [40]. Nrf2 activation is also imperative for the process of drug metabolism via ARE-

mediated enzyme induction [33]. Nrf2 activation has been shown to increase survival rates during sepsis in mice [38]. In the study of some diseases related to oxidative stress, such as Alzheimer's and Huntington's disease, where the administration of antioxidants as treatment has not succeeded; therapeutic alterations to the Keap1-Nrf2 pathway could provide a more effective treatment by activating an innate and continuous antioxidant response [47]. Systemic hyperactivation of Nrf2, however, has the potential to induce detrimental effects. Previous studies have suggested Nrf2 plays a role in chemoresistance, making the treatment of some cancers more difficult [36]. Eliminating all of the ROS in a biological system would greatly impair vital functions like bone marrow homeostasis [36].

1.7.5   Effects of the Keap1-Nrf2 Pathway on Bone

Being ubiquitously expressed, the Nrf2 signaling pathway has the potential to affect all body tissue types, and has recently come into view as a pivotal regulator of bone metabolism [1]. Nrf2 deficient mice have significantly diminished bone strength and impaired bone formation in response to mechanical loading [1]. The loss of mass and strength in Nrf2 deficient mice results from an imbalance in bone remodeling, and suggests that the loss of antioxidant function in female osteoporotic patients may be linked to the Keap1-Nrf2 pathway [1]. Indeed, deletion of Nrf2 has been shown to increase osteoclast number when compared to wild type controls [42], and over activation of Nrf2 resulted in increased levels of RANKL and a consequential suppression of osteoclast activity [1]. Effective control of Nrf2 activation could be invaluable as a preventative measure or therapeutic treatment in bone-related health, as recently illustrated by a study by Katsumata et al, which demonstrated that a known Nrf2 activator, epigallocatechin gallate (EGCG) inhibits osteoclastic absorption associated with degenerative diseases of the teeth and facial bones [49]. This example highlights the importance of maintaining the appropriate balance when dealing with Nrf2 activation, as some level of osteoclastic absorption is necessary for tooth movement during orthodontic treatment [49]. Another natural Nrf2 activator, gastrodin, was recently found to protect against the development of osteoporosis that occurs following prolonged glucocorticoid therapy [50]. The inhibitory effect of Nrf2 activation on osteoclast activity may result from RANK/RANKL levels, actin ring interference, or interaction with NFATc1 [1]. While the bulk of research has been directed at the study of Nrf2 and its effects on osteoclast activity, there is controversial data to suggest the Nrf2 may also play a role in

osteoblast activity [1, 42]. There may be other systemic impacts of Keap1 deficiency that act independently of Nrf2 function, as it has also been suggested recently that Keap1 deficiency may have adverse effects on bone metabolism [51, 52]. This could mean systemic Keap1 deficiency is not an ideal means of activating Nrf2, or that moderate activation is preferential to extreme cases of hyperactivation. Exploring the specific mechanisms at work during Nrf2 signaling provides an opportunity to better understand the mechanisms of bone loss, and may identify effective therapeutic targets for combating bone diseases [1].

1.7.6   Research Goals

Previous findings indicate that Nrf2 activation increases bone formation. The majority of research in this field, however, has used global knockout models of Nrf2 deficiency [1]. The goals of this study were to investigate the effects of Nrf2 activity on bone formation through two specific circumstances. First, the effects of Nrf2 activation via partial Keap1 knockdown on ageing mice were examined; testing our hypothesis that moderate Nrf2 activation improves bone quality by affecting bone metabolism and response to mechanical loading. This study provides potential insights into considerations that should be taken when treating age-related bone diseases such as osteoporosis. Second, the effects of osteocyte-specific deletion of Nrf2 on adult mice were investigated; testing the complementary hypothesis that osteocyte-specific Nrf2 deletion reduces bone quality by affecting bone metabolism and response to mechanical loading. The role of Nrf2 in bone homeostasis has thus far been largely limited to the activity of osteoclasts [1]. This study provides insight into the role of Nrf2 at the cell population level, with regard to the osteocyte – a relatively under-represented cell type.

CHAPTER 2.   MATERIALS AND METHODS

2.1   Experimental Mice

All animal protocols were reviewed and approved by the Indiana University Animal Care and Use Committee (IUACUC). All animals were provided ad libitum access to standard mouse chow and fresh water for the duration of the study. Animals were housed in plastic cages at a temperature of $22 \pm 1 °$ C with a daily light cycle from 6:00 AM to 6:00 PM. Dmp1-8kb-Cre mice possessing a transgene orienting the cre recombinase sequence downstream of the mouse dentin matrix protein 1 (Dmp1) gene with approximately 8 kb of 5' flanking sequence were obtained from IU medical school via Teresita Bellido's research group according to their published protocol [53]. Subjects from a line of mice created by Jingbo Pi's group with LoxP sites flanking the exon of Nrf2 ($Nrf2^{LoxP/LoxP}$) were obtained via Bobby Thomas of the Medical College of Georgia at Augusta University [54]. Keap1 deficient individuals from a strain of Keap1 deficient mice were obtained through Riken BRC (No.RBCRC01388). This strain carries a targeted mutation replacing Keap1 with a cassette encoding neomycin and nls-lacZ (RIKEN BioResource Research Center, Saitama, Japan). All genetics lines used in both studies were derived from C57BL/6J mice (Jackson Laboratories, Bar Harbor, ME, USA).

2.2   Breeding

The targeted mutation line of $Keap1^{+/-}$ mice is maintained by repeated crosses of $Keap1^{+/-}$ animals with C57BL/6J wild-types. This cross generates approximately 50% $Keap1^{+/-}$ offspring and 50% $Keap1^{+/+}$ wild-type littermate controls (Figure 1). Previous analysis of calvarial osteoblasts from this breeding scheme confirmed increased expression of Nrf2 in $Keap1^{+/-}$ animals (Figure 23, Li 2019). Osteocyte-specific deletion of Nrf2 was achieved using a Cre/Lox system of two transgenic lines. Dmp1-8kb-Cre mice (which express Cre recombinase only in the presence of Dmp1 expression) were crossed with $Nrf2^{LoxP/LoxP}$ mice (with LoxP sites flankingthe exon of both copies of the Nrf2 sequence, generating a hemizygous F1 generation. Breeding pairs consisting of two hemizygous mice produce Dmp1-Cre positive offspring. Approximately 25% of the offspring produced are $Nrf2^{Flox/Flox}$, conditionally deleting Nrf2 expression in Dmp1+ cells (i.e. osteocytes). Another ~25% will be wild-type littermate controls ($Nrf2^{+/+}$). The

remaining 50% are expected to be more hemizygous mice that can be used to maintain the colony (Figure 13).

2.3   Genotyping

The genotype of each experimental animal was obtained through polymerase chain reaction (PCR) amplification of DNA samples. Genotyping was performed after weaning the test animals, and repeated after sacrifice for confirmation. DNA was obtained at 3-4 weeks of age through the collection of the 1mm ear notch removed for individual identification. The ear punch was sanitized between animals with 70% ethanol. At sacrifice, samples were obtained by removing the distal 1-2mm of the tail. Scissors were sanitized with 70% ethanol after each tail snip. These samples were placed into individually labeled 1.5 mL centrifuge tubes. Samples were processed immediately after collection. Lysis buffer consisting of: 50 mM Tris (pH 8), 50 mM KCl, 2.5 mM EDTA, 40 mM 0.4% NP, 40 mM 0.45% Tween, and 2.5mM 4% Proteinase K (10 mg/mL) was mixed immediately prior to use. For tail tip or ear notch samples, 100 µL or 30 µL of this lysis buffer was added, respectively. The 1.5 mL centrifuge tubes were then left in a water bath at 56°C overnight. The following morning, all tubes were removed from the water bath and centrifuged, before being placed into a dry bath at 95°C for 10 minutes in order to denature the Proteinase K. The lysates were then diluted with a volume of autoclaved milliQ water equal to the volume of lysis buffer used on that sample, resulting in 60µL ear notch lysates and 200µL tail-tip lysates.

PCR mix was prepared using 12.5 µL per sample of GoTaq® Green Master Mix (Promega Corporation, Madison, WI, USA) held in PCR certified 0.2 mL centrifuge tubes. For every tube, 0.5 µL of each appropriate primer was added. When genotyping for Keap1, a set of three primers was used. The primers and sequences for amplification of Keap1 were as follows: d132 – 5'-CGG GAT CCC CAT GGA AAG CT TAT TGA GTT C-3', TVneo – 5'-TCA GAG CAG CCG ATT GTC TGT TGT GCC CAG TCA-3', and intR – 5'-CAG TTT TCC TCC AGC CTG TC-3' (Figure 2). When genotyping for Dmp1 CRE, a set of two primers was used. The primers and sequences for amplification of Dmp1 CRE were as follows: forward (CsCre1) – 5'-AGG GAT CGC GAG GCG TTT TC-3' and reverse (CsCre2) – 5'-GTT TTC TTT TCG GAT CCG CC-3' (Figure 14A). When genotyping for Nrf2 LoxP, a set of three primers was used. The

primers and sequences for amplification of Nrf2 LoxP were as follows: forward (Nrf2_Loxp1_F) – 5'-CAC AAT GGT ATG CCT GCT GT-3', reverse (Nrf2_LoxP1_R) – 5'-AAG AGG GGG TTG GAA AGA GA-3', and wild-type reverse (Nrf2_LoxP1-WT_R) – 5'-TCT GCA CCA GAG TTC AAA GG-3' (Figure 14B). All primers were obtained through IDT (Integrated DNA Technologies, Inc., Skokie, IL, USA). Next, a volume of sterile PCR water was added to each tube. In cases when two primers were used, 5.5 µL of water was added. When three primers were used, 5.0 µL of water was added. Finally, 1.0 µL of DNA lysate from the appropriate animal was added to each tube, resulting in a consistent volume of 20 µL per tube. All tubes were then loaded into an Eppendorf Mastercycler® gradient thermal cycler (Eppendorf North America, Hauppauge, NY, USA) and run for 40 cycles before a 15°C hold until removal.

Upon completion of PCR, samples were removed from the thermal cycler and added to a 2.5% agarose gel prepared using 1.25 g agarose and 50 mL 0.5x TBE buffer with an added 7 µL of SYBR® Safe DNA gel stain (Thermo Fisher Scientific, Waltham, MA, USA). 10 µL of each post-PCR sample was added to consecutive wells in the gel, flanked by two wells containing 10 µL of Quick-Load® 100 bp DNA Ladder (New England Biolabs, Ipswich, MA, USA) for reference. Immediately following electrophoresis, the gel was imaged using a Typhoon™ FLA 9500 laser scanner (GE Healthcare Life Sciences, Marlborough, MA, USA). When genotyping animals for Keap1, the presence of a single band at 350 bp indicated a Keap1$^{+/+}$ individual. The presence of a single band at 500 bp would indicate a Keap1$^{-/-}$ individual (however, this phenotype is lethal before weaning age and was never observed in this study). The presence of both bands (350 bp and 500 bp) indicated a Keap1$^{+/-}$ individual. When genotyping for Dmp1 CRE, the presence of a band at 300 bp indicated a Dmp1 CRE+ individual. No visible band appeared for Dmp1 CRE- individuals. When genotyping for Nrf2 LoxP, the presence of a single band 180 bp indicated an Nrf2$^{flox/flox}$ individual. The presence of a single band at 210 bp indicated an Nrf2$^{+/+}$ individual. The simultaneous presence of both bands indicated a heterozygous individual with only one LoxP site

2.4   Mechanical Loading

The loading experiment was initiated at 6 months of age for the Dmp1-Cre, Nrf2-LoxP study; and at 18 months of age for the Keap1 heterozygote study group (±14 days). Two weeks prior to

sacrifice, animals were subjected to in vivo axial mechanical loading of the right ulnae once a day for a duration of 3 days. The axial ulnar loading method established by Torrence et al was followed [31]. Thanks to the uniformly curved shape of the ulna, this results in a predictable and repeatable pattern of strain applied to the midshaft without damaging the bones [24]. This loading method is also preferable to four-point bending as it applies the force far enough from the site of strain to eliminate the need for a loading sham group [31]. Instead, the left ulna of each animal serves as a non-loaded internal control. Mice were handled according to the protocol previously used by this lab [32]. Before each session of loading, animals were anaesthetized via inhalation of 2% Isoflurane, USP. The body weight of each individual was recorded. They were then situated into a Bose® ElectroForce® Model 3220 mechanical testing system (TA Instruments, New Castle, DE, USA), which carried out a set of 120 cycles of mechanical strain (2.9 N for males, 2.6 N for females) over the course of 60 seconds. Anesthesia was maintained throughout the procedure using a mouse nose cone. This process was repeated each day until 3 rounds of mechanical bone loading had been completed on each test subject. All animals were allowed normal cage activity following loading sessions. Two days following the third and final round of loading (9 days prior to sacrifice), 0.2 mL of the green fluorochrome label calcein (30 mg/Kg body weight) was administered via intraperitoneal injection. Five days later (4 days prior to sacrifice), 0.2 mL the red fluorochrome label alizarin (50 mg/Kg body weight) was administered via intraperitoneal injection. All test animals were sacrificed 4 days after the administration of alizarin.

2.5 Sacrifice

All test subjects were euthanized at 6 months of age, after completing the 14-day mechanical loading test cycle. In order to obtain a large volume (200-400 µL) blood sample from each individual, animals were first deeply anesthetized using Isoflurane, USP. Sacrifice body weight was recorded. Submandibular blood specimens were then collected and stored in BD Microtainer® blood collection tubes with a serum separating additive (Becton, Dickinson and Company, Franklin Lakes, NJ, USA). Anesthesia was maintained as animals were then euthanized via cervical dislocation. Following euthanasia, several tissues were harvested and processed for storage. The right femur was collected and placed into a glass vial of 10% buffered formalin phosphate. The right tibia was collected, wrapped in a saline-soaked gauze pad, and

sealed into a small plastic bag. The Left femur was collected and placed into a 1.5 mL centrifuge tube. The left tibia was collected and placed into a 1.5 mL centrifuge tube. The spine was collected, wrapped in a saline-soaked gauze pad, and sealed into a small plastic bag. The right and left ulnae were collected and placed into the glass vial of formalin. Using scissors, the distal 1-2mm of the tail was snipped and placed in a 1.5 mL centrifuge tube.

All harvested tissues were then returned to the lab for processing and storage. The blood specimens were centrifuged for 10 minutes to separate the serum before storing at -80°C. The glass vials of formalin containing the right femur and both ulnae were held at 4°C overnight, before replacing the formalin with 70% ethanol and returning to storage at 4°C. Plastic bags containing the spine and left femur samples were stored at -20°C. Centrifuge tubes containing tibiae were stored at -80°C. Tail tips were used to prepare DNA lysates for genotype confirmation.

2.6   Biomechanical Testing and Analysis

The mineral content of the left femur of each test subject was analyzed through dual energy X-ray absorptiometry (DXA) using a PIXImus bone densometer (PIXImus Lunar Corp., Madison, WI, USA), and each femur was imaged with a SkyScan 1172 microCT (SkyScan, Kontich, Belgium) following the protocol previously established [55]. Phantoms were included in each scan. After imaging, a four-point bending test was conducted on each femur. Reconstitution of 3D structure was carried out using NRecon reconstruction software (Micro Photonics Inc., Allentown, PA, USA). CTan software was used to select ROI for each midshaft. The trabecular ROI was defined as 3mm of the trabecular region of the distal femur beginning 1 mm proximal to the growth plate. Reconstructions and four-point bending data were then analyzed through MATLAB®. Cortical ROIs composed of 7 images each averaging 15 μm of cortical bone surface were utilized in this analysis.

2.7   Histology and Histomorphometry

From each experimental animal, the following tissues were processed for histological and histomorphometric analysis: right femur, right ulna, and left ulna. After dissection, these samples were fixed in 10% neutral-buffered formalin (NBF) for 24 hours, followed by storage at 4°C in

70% EtOH until the onset of processing. Processing of the samples consists of two stages: dehydration and infiltration of embedding media. Prior to processing, the femora and ulnae were cleaned of remaining external soft tissue. The radii were removed from all left ulnae, while right radii were left intact to facilitate quick distinction between right and left sections. The left and right ulnae from each experimental animal were then wrapped together at the proximal and distal ends by looping twice with 36 AWG copper wire. The ulna bundles were measured, and the right mid-shaft of each bundle was marked lightly with a pencil. Each completed ulna bundle was placed in a labeled tissue cassette and submerged in 70% EtOH. Each right femur sample was measured, and the mid-shaft lightly marked with a pencil. The marrow cavity of the distal femur was exposed above and below the growth plate by shaving away the patella groove parallel to the diaphysis with a #22 scalpel blade. Each femur was then cut 1.5 mm distal to the mid-shaft mark using a Buehler® Isomet ™ low speed saw (Buehler, Lake Bluff, IL, USA). The distal femur and femur mid-shaft sections were then placed in individually labeled tissue cassettes and submerged in 70% EtOH.

Dehydration was achieved by replacing the 70% EtOH immersing solution with a stepwise series of EtOHs with concentration being increased every 2-8 hours up to 100% EtOH. Once samples were completely dehydrated, the process of infiltration of embedding media was initiated. First, the 100% EtOH was replaced with a 1:1 mixture of EtOH and methyl methacrylate (MMA) for 2-8 hours. Next, this mixture was replaced with undiluted MMA monomer for another 2-8 hours. After that, the undiluted MMA was replaced with infiltration media (MMA and 4% dibutyl phthalate) and samples were placed under a vacuum for 24 hours at 17 inHg. This was then replaced with a freshly mixed volume of infiltration media, and returned to the vacuum at 17 inHg for another 2-7 days. Upon completion of this step, samples were considered fully dehydrated, infiltrated, and ready to embed.

2.7.1   Ulna Sample Preparation

Prior to embedding samples, polymerized bases were prepared in labeled 6x50 mm glass culture tubes using embedding media (MMA, 4% dibutyl phthalate, 0.8% perkadox). A drill was used to create a hole in the center of each polymerized base, which served to hold samples upright in the tube during polymerization. These tubes were nearly filled with embedding media, then each ulna bundle was placed into the corresponding labeled tube. Tubes were stored in a tube rack to

keep them upright; and placed, uncapped, under a vacuum (17 inHg) for at least 20 minutes, before being tightly capped with rubber stoppers. Sealed tubes were placed into 1 oz plastic vials filled partially with distilled water. These vials were left on a slide warmer at 25° C for 1-2 days, then heat cured overnight at 60° C. The glass was removed from the completed MMA tubes using a hammer.

Using a wire saw, 5 sequential transverse thick sections (approximately 50 µm) were collected, beginning 2.5 sections before the mid-shaft pencil mark to ensure mid-shaft collection. These sections were sonicated to remove sawdust, then left to dry at room temperature overnight. Dry sections were mounted to clean microscope slides using Eukitt® mounting medium (MilliporeSigma, St. Louis, MO, USA). A small piece of paper towel was placed between this section and a second microscope slide, and a binder clip was used to hold the two slides together overnight. The following day, the top slide and paper towel were removed. The mounted section was covered in several dropped of xylenes-thinned mounting medium (filling gaps and increasing surface area for grinding the section). These slides were left to dry at room temperature overnight. Dried coated slides were then ground to a thickness of 30-50 µM. This was achieved by holding each slide with a small suction cup and gently sanding, section down, in a figure-eight motion against wet 600 grit sandpaper. Ground slides were sonicated in distilled water and left to dry overnight. The following day, a glass cover slip was applied to each slide using xylenes-thinned mounting medium. After drying overnight, completed slides were stored in a slide box.

2.7.2   Femur Midshaft Slide Preparation

Preparation of right femur mid-shaft samples closely followed the same protocol used for ulna cortical sections. The protocol only differed in the number of sections collected with the wire saw. For femur mid-shaft samples, 3 sequential 50 µM transverse sections were collected, beginning 1.5 section widths prior to the mid-shaft pencil mark to ensure mid-shaft collection.

2.7.3   Distal Femur Slide Preparation

The right distal femur of each test animal was embedded in 1 oz plastic vials using embedding media. Prior to adding the samples, bases were polymerized in each vial using 6 mL of embedding media. Vials with prepared bases were labeled for each sample and filled with

embedding media. Each fully infiltrated distal femur was removed from a tissue cassette and quickly placed into the corresponding labeled vial. Uncapped vials were placed in a vacuum (17 inHg) for at least 2 hours. Vials were then capped tightly and refrigerated at 4° C overnight. Further polymerization was carried out at room temperature. The samples, now embedded in blocks of MMA, were removed from their molds using a hammer and chisel.

Blocks of MMA containing embedded distal femora were trimmed and shaped using a saw and grinder. Portions of the MMA were cut away in order to form an equiangular rectangle with the tissue sample centered 0.5 cm from all sides and flush with the front face of the block. The outside edges of the front face of each block were then rounded out with the grinder to reduce tears or snags during thin sectioning. Thin sectioning of the finished blocks was carried out on a rotary microtome using a tungsten carbide knife. After securing a block to the microtome and softening the face with 50% EtOH, a series of 4 µm thick longitudinal sections were taken from the block face and transferred to Superfrost® Plus microscope slides subbed with a 1% gelatin solution (Thermo Fisher Scientific, Waltham, MA, USA). Five slides were prepared for each tissue sample, with each slide containing three sequential sections. After three sections had been transferred to a slide, it was flooded with 70% EtOH and each section was gently smoothed with a small paintbrush to reduce wrinkles and folds. The slide was then covered in plastic and excess EtOH was gently removed by placing bibulous paper over the plastic and rolling across the slide with a rubber roller. When a set of five slides had been completed for a sample, the slides were sandwiched between two blank microscope slides and secured together with a binder clip. These stacks were left to dry overnight at 37° C. The following day, the clips and plastic were removed and slides were stored in a slide box.

2.7.4 Histological Staining

One slide containing 3 thin trabecular sections of the distal femur of each test subject was TRAP stained. This stain can be used as a histologic marker, as all osteocytes express and secrete tartrate-resistant acid phosphatase (TRAP) [9]. Toluidine blue was used as a counterstain. Static histomorphometry of stained slides was carried out using OsteoMeasure™ histomorphometry software (OsteoMetrics, Decatur, GA, USA). Slides were analyzed under bright-field illumination on an Olympus DP72 digital microscope camera connected to an Olympus BX53 Telepathology Microscope System (Olympus Scientific Solutions Americas, Waltham, MA,

USA). Each sample was scored for the following parameters: osteoclast number (N.Oc), osteoclast surface (Oc.S/BS), osteoclast number over bone surface (N.Oc/B.Pm), and osteoclast number over perimeter (N.Oc.Oc.Pm).

2.7.5 Dynamic Histomorphometry

Quantitative analysis of bone samples was achieved using OsteoMeasure^{TM} histomorphometry software (OsteoMetrics, Decatur, GA, USA). Slides were analyzed on an Olympus DP72 digital microscope camera connected to an Olympus BX53 Telepathology Microscope System (Olympus Scientific Solutions Americas, Waltham, MA, USA). Fluorochrome labels were visualized through illumination with an X-Cite Series 120Q fluorescence illuminator (Excelitas Technologies, Waltham, MA, USA). Measurements were taken on a Wacom touchscreen monitor with stylus through the tracing of focused, illuminated sections at 200x magnification (Wacom, Kazo, Saitama Prefecture, Japan).

Unstained cortical sections of the left and right ulnae of each test animal were scored for the following direct measurements: periosteal perimeter, endocortical perimeter, periosteal single label, endocortical single label, periosteal double label, and endocortical double label. Derived measurements including MS/BS, MAR, and BFR/BS were calculated using these primary tracings. An unstained right femur midshaft cortical section from each test animal was also scored for the same set of parameters as the ulnae.

Because only the right ulna of each animal was loaded, each left ulna could be used as a non-loaded control against the reciprocal section from the right ulna. The difference between right and left ulna measurements were calculated and referred to as the relative values, which represent the amount of metabolic bone activity occurring as a direct result of mechanical loading [32]. These relative values illustrate loading-induced bone formation as a measure of mechanotransduction.

Two trabecular sections from the right distal femur of each mouse were scored. One unstained section was scored for trabecular surface and fluorochrome labeling, and derived kinetic indices including BV/TV, MS/BS, MAR, and BFR/BS were calculated using the direct tracings. A TRAP stained section was used to measure osteoclast number, osteoclast surface, and proportional trabecular bone surface.

2.8   Statistical Analysis

All data are reported as mean ± standard error of the mean (SEM). Potential outliers were identified using the interquartile range method, a resistant method of statistical analysis which prevents outliers from skewing overall results [56]. Selected parameters for the identification of potential outliers were periosteal BFR and trabecular BV/TV. After investigating potential outliers, one sample from the Keap1 aging study was determined to have extremely anomalous bone characteristics and was subsequently omitted from statistical analysis. Test groups were compared using a two-tailed Student's t-test of two groups assuming unequal variances using Excel software. Significance was determined as $p < 0.05$.

CHAPTER 3.   RESULTS

3.1   Moderate Nrf2 Activation via Partial Deletion of Keap1 in Aging Mice

3.1.1   Keap1$^{+/-}$ Mice

At 18 months of age, study animals were selected from the breeding line described previously. After excluding one identified outlier, 2 female Keap1$^{+/+}$ (WT), 14 female Keap1$^{+/-}$ (HT), 7 male Keap1$^{+/+}$ (WT), and 12 male Keap1$^{+/-}$ (Ht) mice were utilized for statistical analysis. At the start of the loading study, female Ht mice weighed less than WT controls (-24% p = 0.008). As WT females lost slightly more weight over the course of the study than Ht females, no such difference was recorded when comparing the final body weights of Ht and WT females. All mice lost an average of 0.86 grams over the course of the loading study, although none of the losses reached significance. While males weighed significantly more than females (+15% p = 0.003), there were no significant differences in average weight change between HT animals and their WT controls. (Figure 3)

3.1.2   Biomechanical Properties

Structural and material properties of bone quality were assessed through PIXImus analysis and subsequent 4-point bending test of the left femur of each test subject.

3.1.2.1   PIXImus Analysis

Keap1$^{+/-}$ female mice were found to have decreased bone mineral density (-13% p = 0.0004) versus wild-type females. No genotype specific differences were found between male Keap1$^{+/-}$ mice and wild type controls. Overall, males had 13% higher BMC (p = 0.003) and 7% higher BMD (p = 0.01) than females (Figure 6).

3.1.2.2   Mechanical Testing: 3-Point Bending

No significant differences were observed between the biomechanical properties of Keap1$^{+/-}$ and their wild-type controls for either male or female animals. When examining structural properties, female stiffness was 28% higher than that of males (p = 0.004), and male ultimate force was 20% higher than that of females (p = 0.005). This did not result in any significant difference in total

work between males and females and was not genotype specific. When examining the bone's material properties, females were found to have 44% higher Young's Modulus compared to males (p = 0.0002). No sex or genotype specific differences in toughness or ultimate stress were observed (Figures 4-5).

3.1.2.3   Trabecular analysis

Trabecular analysis found that Keap1$^{+/-}$ males had significantly higher trabecular numbers than WT males. There was no significant difference found between heterozygous and wild-type mice in structure model index, trabecular thickness, or trabecular separation. No difference was found in overall BV/TV based on either genotype or sex. Males had higher BV/TV and trabecular number than females, while females had greater trabecular separation (Figure 10).

3.1.3   Histomorphometry

3.1.3.1   Static histomorphometry

To investigate levels of resorptive activity on the trabecular surface, TRAP stained thin sections of the distal femur were scored. There were no significant differences in osteoclast number (N.Oc) observed between Keap1$^{+/-}$ animals and their wild-type controls. Males overall had significantly greater numbers of osteoclasts than females (+65% p = 0.006), but this difference was not genotype specific. There were no differences observed between Keap1$^{+/-}$ individuals and wild-type controls for the parameters of: osteoclast surface (calculated as proportion of bone surface), osteoclast number proportional to bone surface, or osteoclast number over perimeter. For those three parameters, there was also no significant difference in mean values between males and females (Figure 8).

3.1.3.2   Dynamic histomorphometry

Fluorescence scoring of thin trabecular sections of the distal femur showed no significant differences in MS/BS, MAR, or BFR between Ht animals and WT controls. There was also no difference found in these values between males and females. Trabecular BV/TV was 84% higher in males than females (p = 2.45 x 10^{-5}), but this difference was not genotype specific (Figure 9).

Dynamic histomorphometry of cortical left and right ulna sections were used to measure loading-induced bone formation. No significant differences were observed between Keap1$^{+/-}$ animals and

wild type controls regardless of sex for any of the derived indices of: relative MS/BS, relative MAR, or relative BFR (Figure 7).

Unstained cortical sections of the femur midshaft were scored for bone surface as well as periosteal and endocortical fluorescent labeling. Ht females had decreased Ct.T.Ar (-13% p = 0.0003) and Ct.B.Ar (-18% p = 0.006) compared to WT females. However, there was no difference in BV/TV between Ht animals and WT controls. Overall, males exhibited higher Ct.T.Ar (+9% p = 0.001), Ct.B.Ar (+15% p = 4.22 x 10^{-5}), and BV/TV (+7% p = 0.008) than females, but this was not genotype specific. No differences based on genotype or sex were found regarding Ps.MS/BS. Ht females had 57% higher Ps.MAR than WT females (p = 0.02). Ht females also had increased Ps.BFR/BS compared to WT females (+62% p = 0.03). Females overall had higher Ps.MAR (+54% p = 0.02) and Ps.BFR/BS (+60% p = 0.028) than males. No differences based on genotype or sex were detected when analyzing Ec.BFR/BS (Figures 11-12).

3.2   Osteocyte-Specific Deletion of Nrf2 in Adult Mice

3.2.1   Nrf2 cKO Mice

Following the Cre-Lox breeding scheme previously described, male and female Dmp1-Cre$^+$, Nrf2$^{flox/flox}$ (cKO) as well as Dmp1-Cre$^+$, Nrf2$^{+/+}$ (WT) controls were obtained and aged to 6 months. In total, 8 WT female, 15 cKO female, 12 WT male, and 8 KO male mice were utilized for this study. When assessing phenotypic differences in these mice, males were found to have higher body weights at the onset of the loading study (+17% p = 0.0007) compared to females. This 17% increase in weight was consistent with measurements recorded upon completion of the study, immediately prior to sacrifice (p = 6.13 x 10^{-7}). There was no significant difference in weight between cKO animals and their WT controls, for either females or males. Conditional knockout mice were not visually distinguishable from their wild-type controls. Study animals lost an average of 0.17 grams over the course of the study. This change was not sex or genotype specific (Figure 15).

3.2.2   Biomechanical Properties

Structural and material properties of bone quality were assessed through PIXImus analysis and subsequent 4-point bending test of the left femur of each test subject.

3.2.2.1 PIXImus Analysis

No differences in BMD were seen between cKO animals and their WT controls for either females or males. Male mice exhibited a trend toward lower BMD than that of females, but did not reach the level of statistical significance (p = 0.052). Likewise, no genotype specific differences were recorded in BMC for either females or males. BMC values recorded were consistent between males and females (Figure 18).

3.2.2.2 Mechanical Testing: 3-point Bending

No significant differences were observed between the biomechanical properties of cKO animals and their wild-type controls for either male or female mice. When examining structural properties, female stiffness was 20% higher than that of males (p = 4.5×10^{-8}), and female ultimate force was 16% higher than that of males (p = 6.99×10^{-5}). This did not result in any significant difference in total work between males and females and was not genotype specific. There was an insignificant trend towards increased total work in cKO females compared to WT females. When examining the bone's material properties, females were found to have 14% higher ultimate stress (p = 0.0014) and 19% higher Young's Modulus (p = 0.008) compared to males. No sex or genotype specific differences in toughness or ultimate stress were observed, but there was an insignificant trend towards increased toughness in cKO females compared to WT females (Figures 16-17).

3.2.2.3 Trabecular Analysis

Trabecular analysis revealed that female cKO mice had decreased trabecular thickness than WT controls (-13% p = 0.027). No significant differences were found between conditional knockouts and wild-type controls in trabecular number, trabecular separation, structure model index, or BV/TV. Male mice had higher trabecular number, trabecular thickness, and BV/TV than female mice. Females had a higher structure model index (Figure 22).

3.2.3 Histomorphometry

3.2.3.1 Static Histomorphometry

TRAP staining of 4 μm sections of the distal femur of each test animal showed no significant differences between cKO and wild-type animals for any of the following parameters: osteoclast

number, osteoclast surface over bone surface, osteoclast number over tissue area, osteoclast number over bone perimeter, or osteoclast number over osteoclast perimeter. Males overall had 28% more osteoclasts in total (p = 0.0002), but those osteoclasts were smaller than those of female mice (males + 15.4% N.Oc/Oc.Pm, p = 7.14 x 10^{-5}). Females had the greater proportion osteoclast surface relative to bone surface (+22% p = 4.02 x 10^{-6}).

3.2.3.2   Dynamic Histomorphometry

Dynamic histomorphometry of the distal femur trabeculae revealed that cKO females exhibited a 33% decrease in MAR (p = 0.04) and a 43% decrease in BFR (p = 0.02) compared to WT female controls. Females had significantly higher BFR (+34% p = 0.002) than males. Males had 44% greater BV/TV than females (p = 4.4 x 10^{-7}). There was no significant change in BV/TV between cKO animals and WT controls (Figures 20-21).

Relative values of fluorescent labeling (calcein and alizarin) of the high-strain region of cortical sections from the midshaft of both left and right ulnae revealed no significant difference in rMS/BS, rMAR, or rBFR for either males of females. Male cKO animals neared significance in their decreased rMAR (p = 0.0517) and rBFR (p = 0.052). There was also no significant difference recorded between male and female relative values (Figure 19).

CHAPTER 4.   DISCUSSION

4.1   Moderate Nrf2 Activation via Partial Deletion of Keap1

The results of this study suggest a subtle sex-dependent effect of the moderate Nrf2 activation resulting from partial deletion of its sequestering protein Keap1 on female bone metabolism, which does not impact mechanotransduction. Female Keap1$^{+/-}$ mice weighed less than their wild-type controls at the onset of this study and were also found to have smaller cortical femur midshaft areas than wild-type females. Although their bodies and bones were smaller than those of their wild-type counterparts, female Keap1$^{+/-}$ mice had no significant decrease in any measured parameter of bone quality.   Female Keap1$^{+/-}$ mice also had 57% higher periosteal MAR and 62% higher periosteal BFR/BS than wild-type controls. This suggests that Keap1$^{+/-}$ females have increased osteoblast activity which effectively maintains equivalent bone quality and strength when compared to wild-type controls, despite their decreased bone size. No genotype specific differences were found in any of the following indices: biomechanical properties, loading-induced bone formation, osteoclast recruitment or activity, or trabecular bone formation. All of these results were unique to females, while male Keap1$^{+/-}$ animals consistently showed no significant differences from wild-type males.

Several differences were observed between male and female mice. Males weighed 15% more than females. Males also had larger femur midshaft areas than females, and higher average BMD and BMC. When assessing structural properties of bone, females had higher stiffness, and males had higher ultimate force. As for the material properties of bone, females were found to have a higher Young's Modulus value. Males had a greater number of osteoclasts than females. Males also had 84% higher trabecular BV/TV than females. However, none of these differences were genotype specific.

It is possible that the Keap1$^{+/-}$ model is subject to systemic effects of the global partial deletion of Keap1, which may serve as a potential influence on bone metabolism. This would coincide with some of the findings of recent studies attributing detrimental phenotypic impacts to Keap1 deficiency [51, 52]. It is also difficult to determine whether these data illustrate that partial Keap1 deletion has no effect on mehcanotransduction, or that any effect was simply

unquantifiable due to the overshadowing effects on aging on mehcanotransduction. Scientific opinion regarding the specific effects of aging on mehcanotransduction are widely varied and poorly understood [10]. The relative bone formation data recorded following mechanical loading suggest that aging may diminish mechanosensitivity, as the wild-type animals used in this study exhibited a low response to mechanical loading. However, due to the low loading response of wild-type animals, the particular load cell used for this study should be recalibrated before repeated trials. Finally, the animal sample used for this study may have been impacted by the variations in mortality among Keap1$^{+/-}$ and wild-type mice. 45% of the Keap1 colony died of natural causes before reaching 1.5 years of age. 87.5% of the animals lost were wild-types, with drastically decreased mortality in the Keap1$^{+/-}$ group. This may have resulted in a control group which inadvertently selected for the strongest and healthiest wild-type animals. Studies from this lab, with results currently in review, using the same RBRC01388 line of mice have found that Keap1 deletion resulted: in increased bone mass (Figure 24, Li 2019), suppressed trabecular osteoclast activity (Figure 26, Li 2019), and increased periosteal BFR in adult mice (Figure 25, Li 2019). These results were sex specific, with the only significant differences being observed in male animals. The divergent results of this current study suggest that aging may introduce interacting factors which complicate the Keap1-dependent response.

4.2 Osteocyte-Specific Deletion of Nrf2 Elicited Mixed Responses in the Bone Metabolism of Adult Mice.

The results of this study suggest an important role of Nrf2 in the osteocyte which affects bone metabolism in varied, sex-dependent ways. Conditional knockout (cKO) mice did not show any visual differences from their wild-type controls. Males were significantly larger than females overall. Female cKO animals exhibited a significant decrease in trabecular MAR and BFR compared to WT controls, suggesting decreased osteoblastic activity in the female conditional knockout. In male trabecular sections, MS/BS, MAR, and BFR were consistent between cKO and WT animals. Although females had significantly higher rates of bone formation, males maintained significantly higher BV/TV than females. There was no genotype specific effect on BV/TV for male or female mice. These results suggest that osteocyte-specific deletion of Nrf2 may inhibit bone formation in females, but not in males.

Bone formation following repeated dynamic ulnar loading did not indicate any significant change in mechanotransduction based on genotype. 48% of study animals showed no difference in MAR between R and L ulnas, suggesting no bone formation response to mechanical loading. Because this inconsistency in the data set led to an extremely wide variance of BFR values for all four groups of this study, it is not surprising that no statistically significant results were obtained. Given the markedly low response to loading, even in wild-type animals, it is possible that loading was unsuccessful. Repeated loading studies should be conducted after a recalibration of the load cell in order to confirm or deny this possibility. Although no statistically significant differences were indicated from these data, cKO male mice appeared to have reduced relative BFR which very nearly reached the level of statistical significance ($p = 0.052$). The statistical power of this study could be increased by subsequent trials.

Deletion of Nrf2 in osteocytes of adult mice impacted several facets of bone metabolism and varied widely based on sex. This suggests a possible sex related variable, such as hormone levels, could impact the interactions between Nrf2 and the osteocyte.

4.3   Future Direction of Research

These studies have provided the basis and motivation for several avenues of future research. The results of the aging study on Keap1$^{+/-}$ mice suggest that a global partial deletion of Keap1 may not be sufficient to impact bone metabolism or mechanotransduction in advanced age, but that moderate activation of Nrf2 does have several relevant effects on bone metabolism. Future studies utilizing this mouse model should increase the sample size and allow for significant age-related mortality, especially of wild-types, in order to increase the statistical power of the results. Then, it could be possible to parse out any small impacts of the partial deletion of Keap1 which may exist. Another avenue of research should utilize a floxed mouse model with a targeted knockout of Keap1 in only a desired tissue of interest. This refined model would likely magnify the results by allowing for a complete deletion in one specific tissue rather than a partial deletion globally. This method would also enhance future results by eliminating much of the systemic effects of global Keap1 deletion that may have interacted with the bone analyzed in this study. The effects of Keap1 deletion specific to the osteocyte, osteoblast, and preosteoblasts could be explored in this way.

APPENDIX

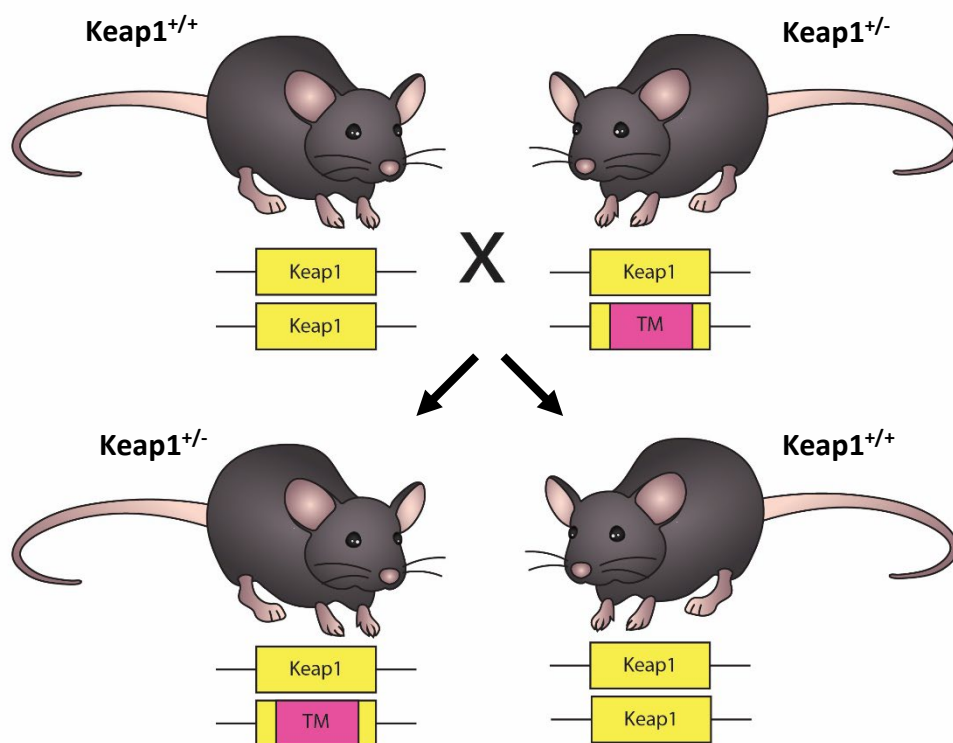**FIGURES: Study 1 – Partial deletion of Keap1 in aging mice**

Figure 1. **Breeding Scheme for Generating Keap1$^{+/-}$ Mice and Wild-Type Littermate Controls.** (A) RBRC01388 mice with one copy of targeted mutation replacing Keap1 are crossed with C57BL/6J wild-type mice, generating Keap1$^{+/-}$ mice and Keap1$^{+/+}$ (wild-type) littermate controls.
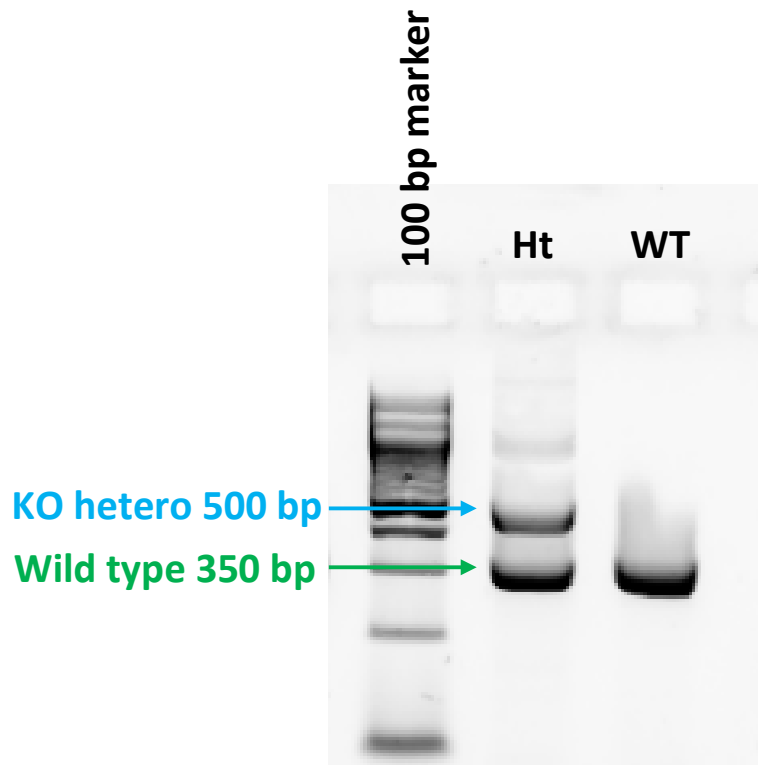
Figure 2.**Keap1 Genotyping.** Electrophoresis gel image displaying amplified bands used to genotype Keap1$^{+/-}$ animal and wild-type controls.

A

Initial Body Weight

B

Final Body Weight

C

Change in Body Weight
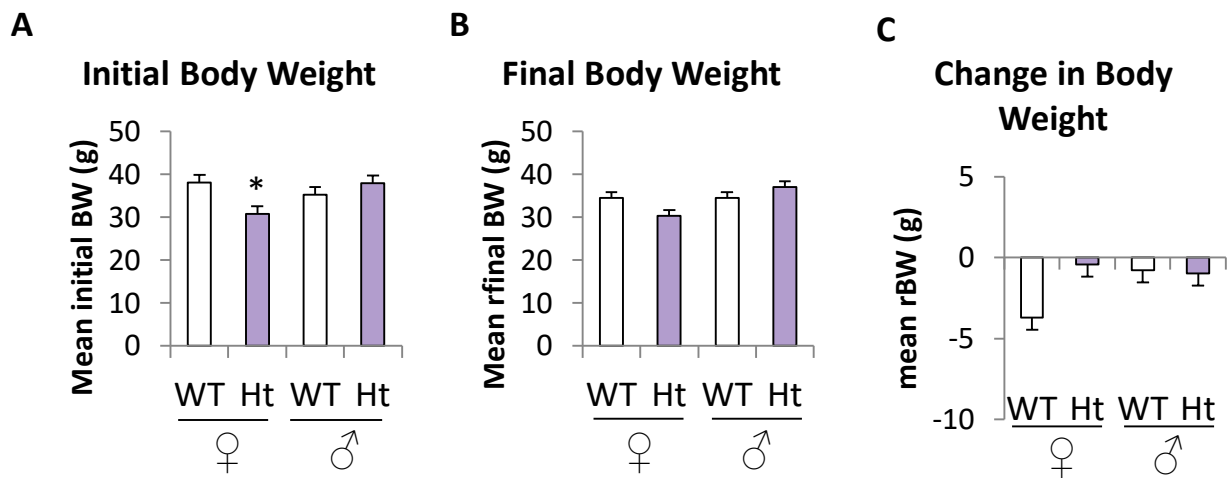
Figure 3. **General Characteristics of Keap1 Heterozygotes.** Keap1^{+/-} females weighed less than WT controls at the onset of the study, but not upon its completion. (A) Initial BW recorded immediately prior to the first round of ulnar loading. (B) Final BW recorded immediately prior to sacrifice. (C) Relative change in BW (rBW) calculated as the difference between final and initial BW.

A
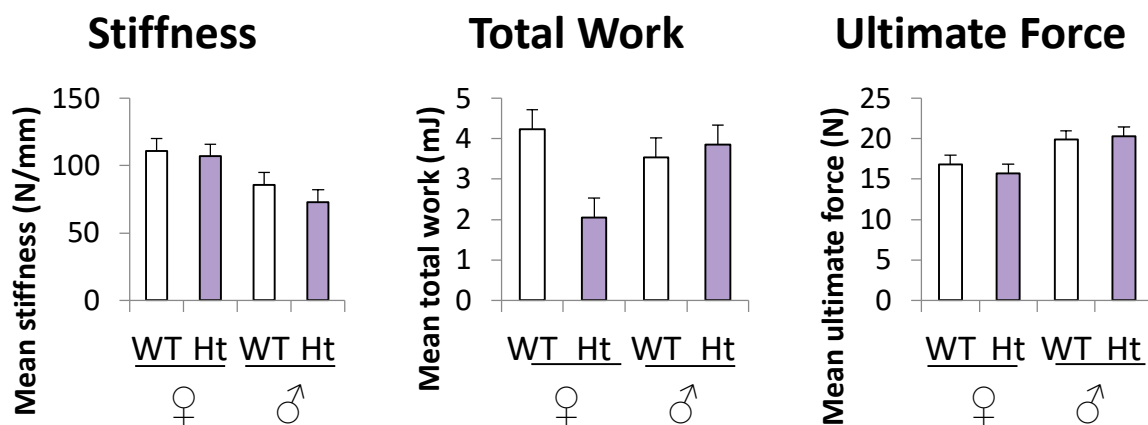
B
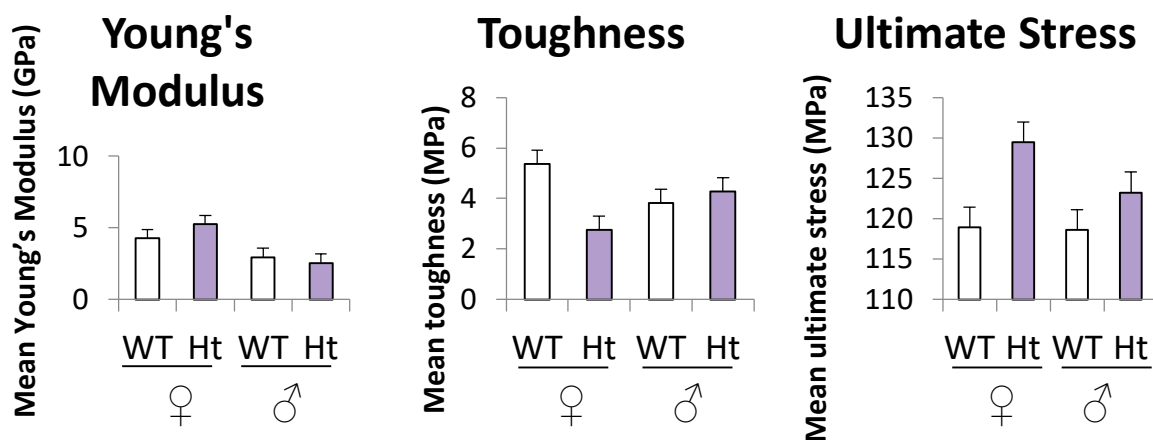
Figure 4. **Biomechanical Property Analysis of Keap1 Heterozygotes.** (A) Structural properties. Nrf2 activation via partial deletion of Keap1 in aged mice did not affect bone stiffness, ultimate force, or total work. (B) Material properties. Partial Keap1 deletion had no significant effect on Young's Modulus, toughness, or ultimate stress. Data were collected through a 3-point bending test of femora from male and female Keap1^{+/-} (HT) mice and wild-type (WT) controls.

A

B
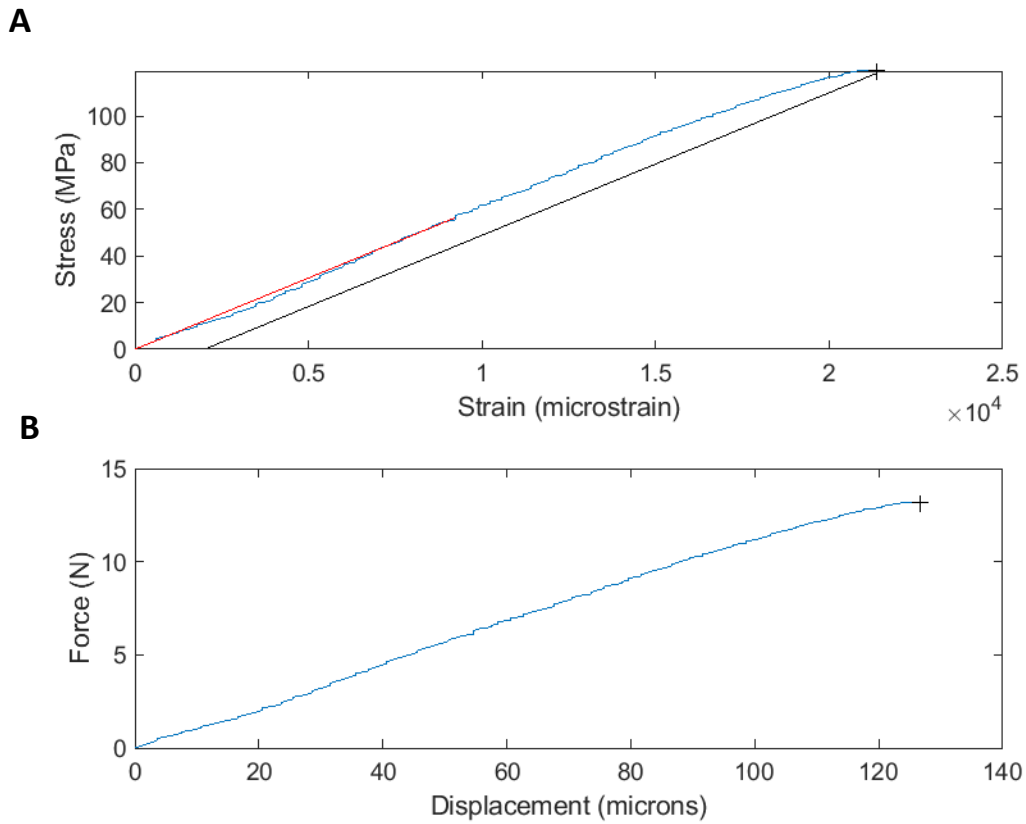
Figure 5. **3-Point Bending of Keap1 Heterozygotes.** An example (A) Stress/strain curve and (B) force/displacement curve illustrating the 3-point bending test of a Keap1$^{+/-}$ mouse femur.

A

Bone Mineral Density

B

Bone Mineral Content
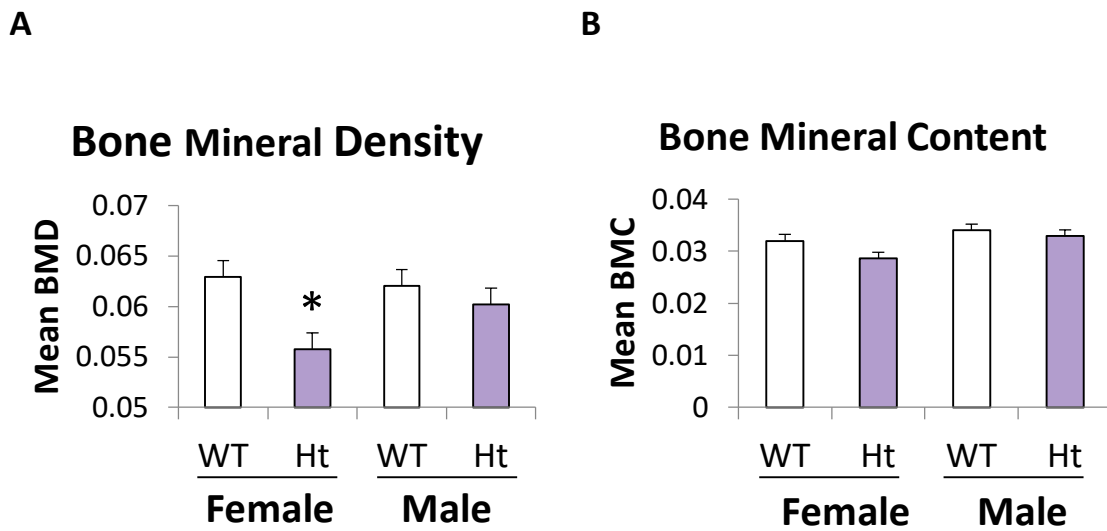
Figure 6. **PIXImus Analysis of Keap1 Heterozygotes.** Group average values for (A) BMD and (B) BMC. Data collected from PIXImus mouse densitometer scans of femora from male and female Keap1$^{+/-}$ (HT) mice and wild-type (WT) controls. Note that *: $p < 0.05$.

rPs.MS/BS

Mean

10
5
0
-5
-10

WT Ht WT Ht
♀ ♂

rPs.MAR

Mean

0.3
0.2
0.1
0
-0.1

WT Ht WT Ht
♀ ♂

rBFR/BS

Mean

20
10
0
-10

WT Ht WT Ht
♀ ♂

	Right Ulna	Left Ulna
WTF		
HtF		
WTM		
HtM		

100 µm
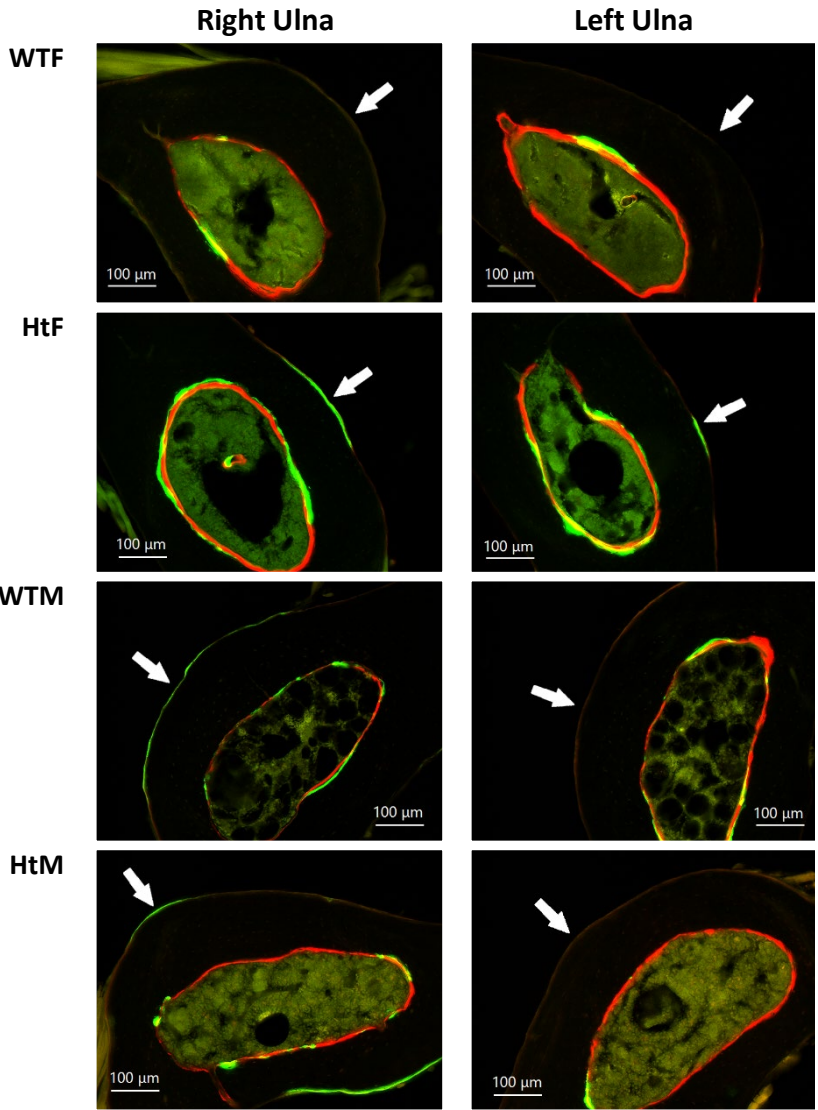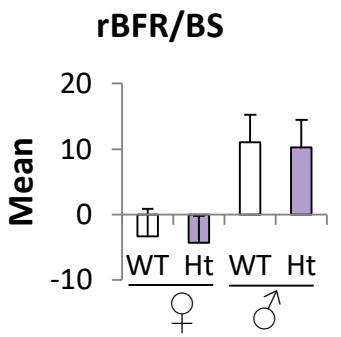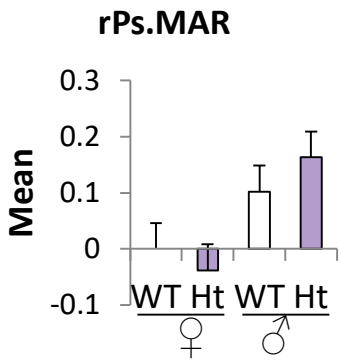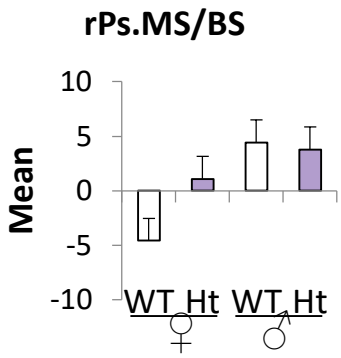
Figure 7. **Loading-Induced Bone Formation in Keap1 Heterozygotes.** (A) The relative values, calculated as the difference between the right (loaded) and left (non-loaded) ulnae were calculated to evaluate bone formation activity as a direct result of mechanical loading. (B) Example photos of cortical sections of right and left ulnae from all four test groups. Note that: white arrows indicate the medial surface of the midshaft, where the highest loading strain is applied; bar = 100μm.
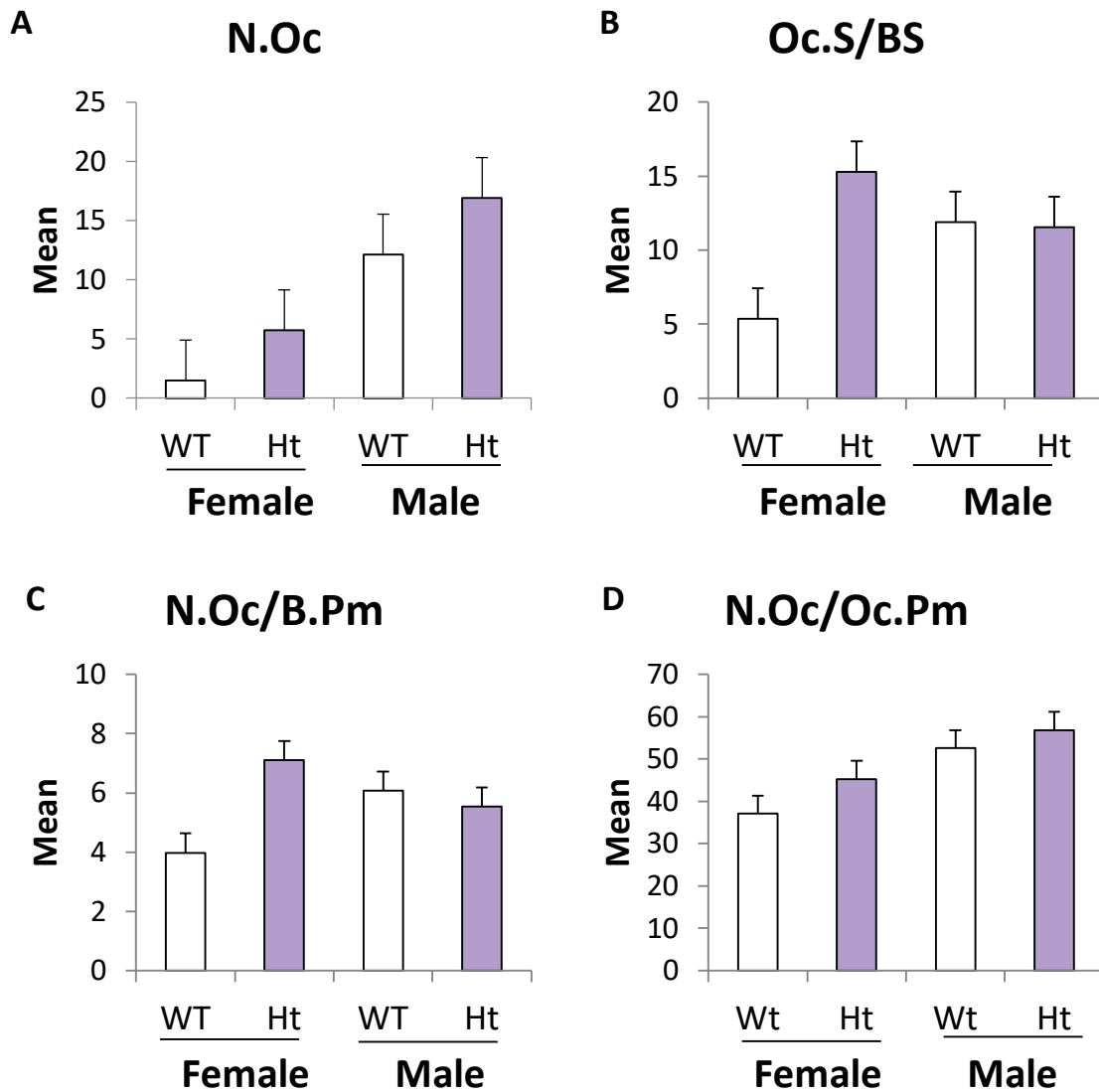
Figure 8. **TRAP Staining Analysis of Keap1 Heterozygotes.** TRAP stained thin trabecular sections of the distal femora of Keap1$^{+/-}$ (HT) animals were compared to those of wild-type (WT) controls. No significant difference was found in any measured parameter including: (A) total osteoclast number, (B) osteoclast number proportional to bone surface, (C) osteoclast surface, or osteoclast number proportional to osteoclast perimeter.
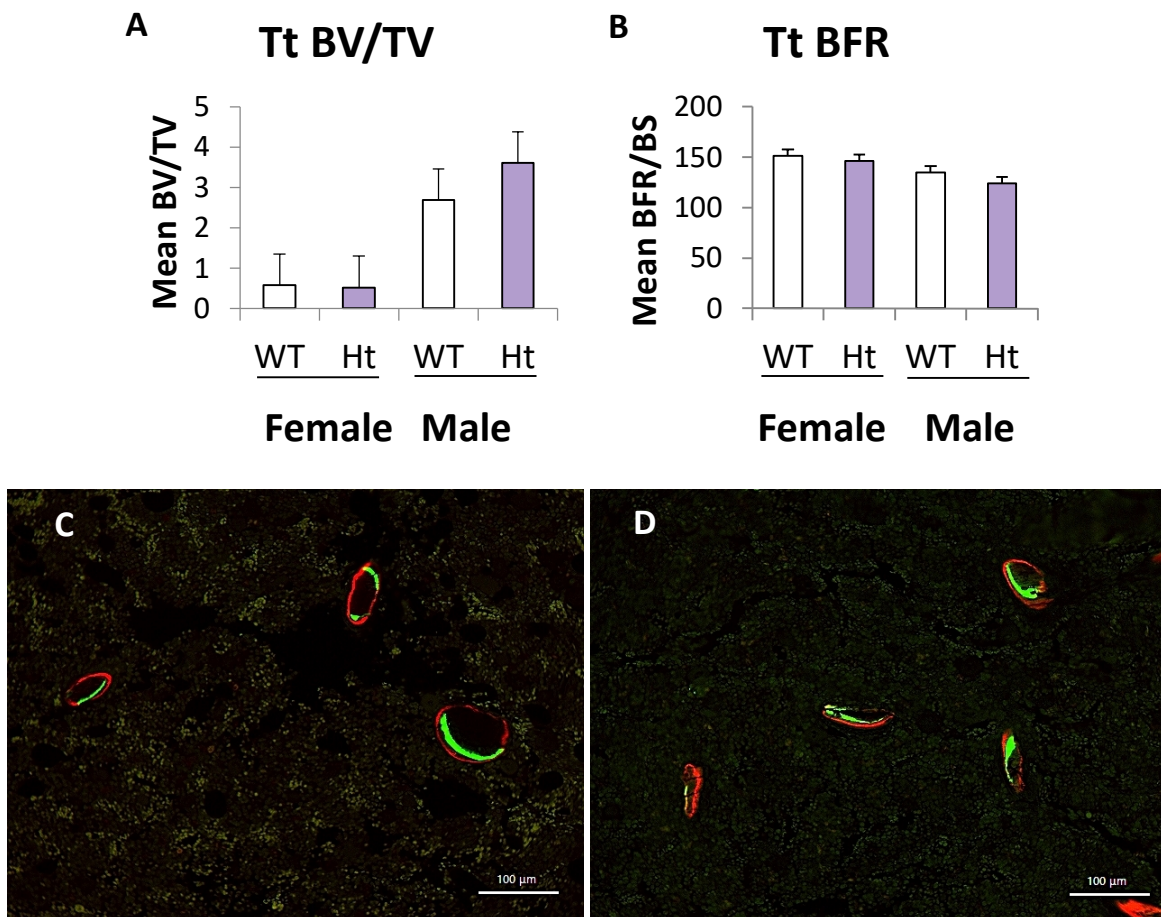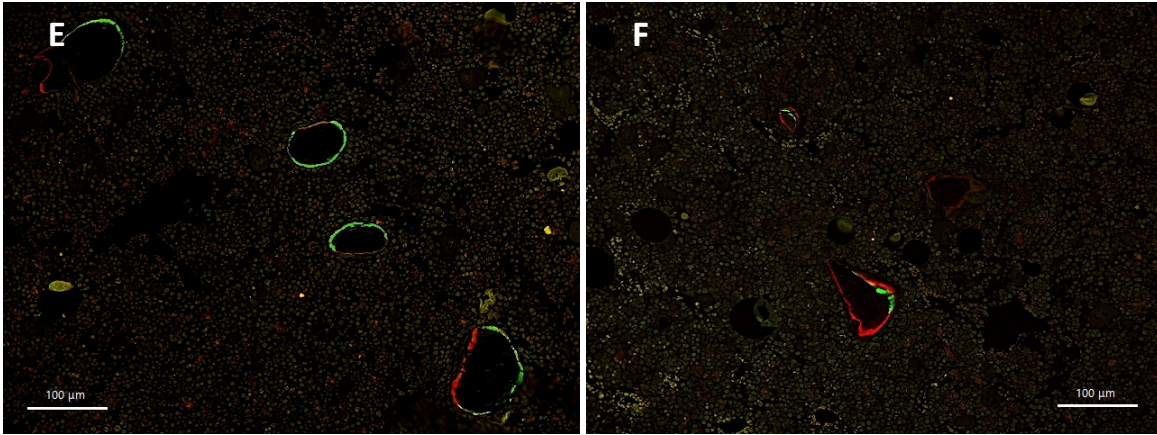
Figure 9. **Dynamic Histomorphometry Analysis of Distal Femur Trabeculae in Keap1 Heterozygotes.** Group averages for (A) Trabecular BV/TV and (B) Trabecular BFR. Photo examples show trabecular fluorescent labeling in (C) wild-type female, (D) Keap1$^{+/-}$ female, (E) wild-type male, and (F) Keap1$^{+/-}$ male mice. Measurements collected from distal femora of male and female Keap1$^{+/-}$ mice and wild-type controls. Note that bar = 100µm.
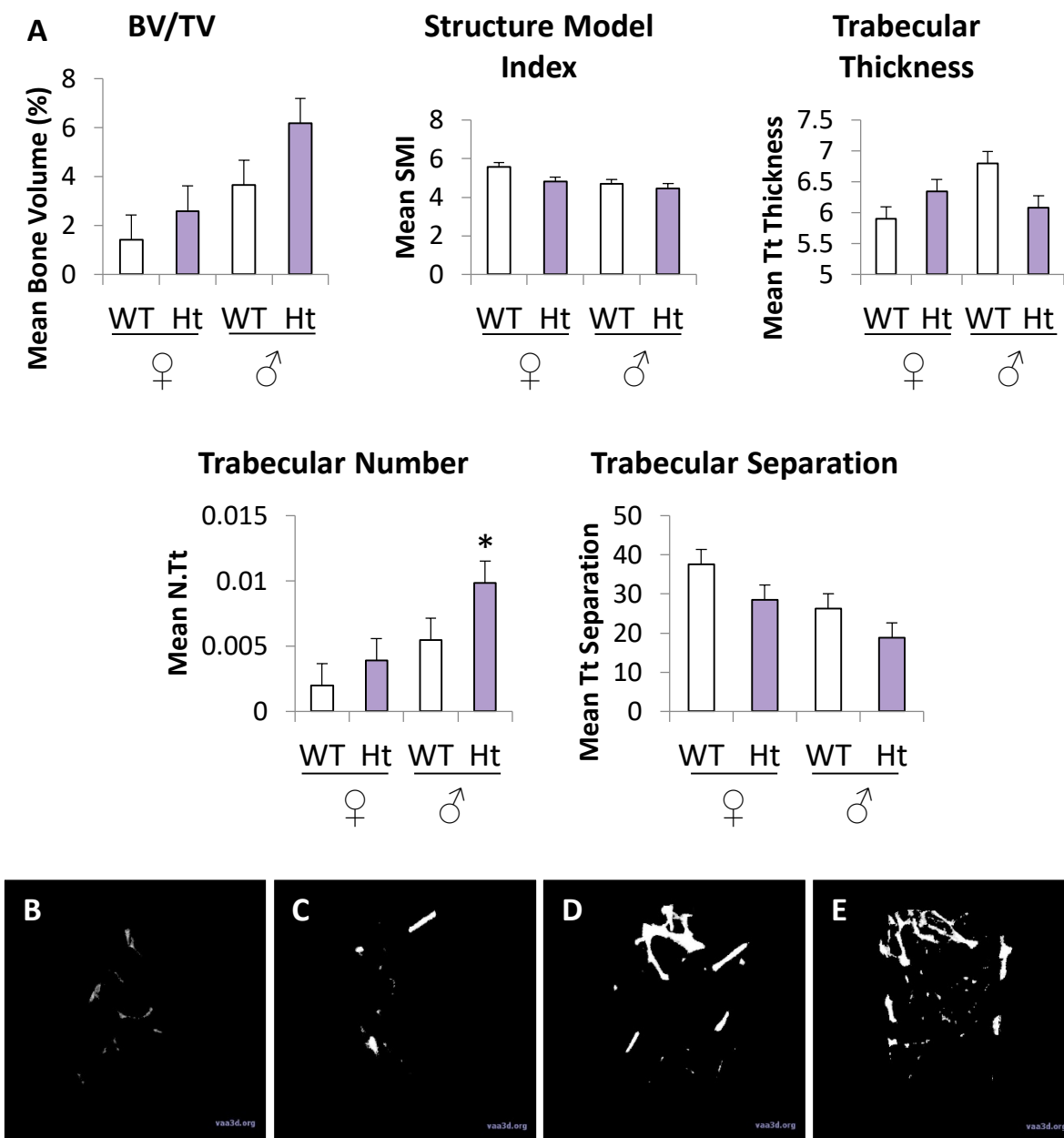
Figure 10. **Trabecular Analysis of Keap1 Heterozygotes.** (A) Trabecular analysis results for distal femur of male and female Keap1^{+/-} mice and wild-type controls; accompanied by 3D reconstructions of trabeculae from (B) wild-type female, (C) Keap1^{+/-} female, (D) wild-type male, and (E) Keap1^{+/-} male mice. Note that *: $p < 0.05$.
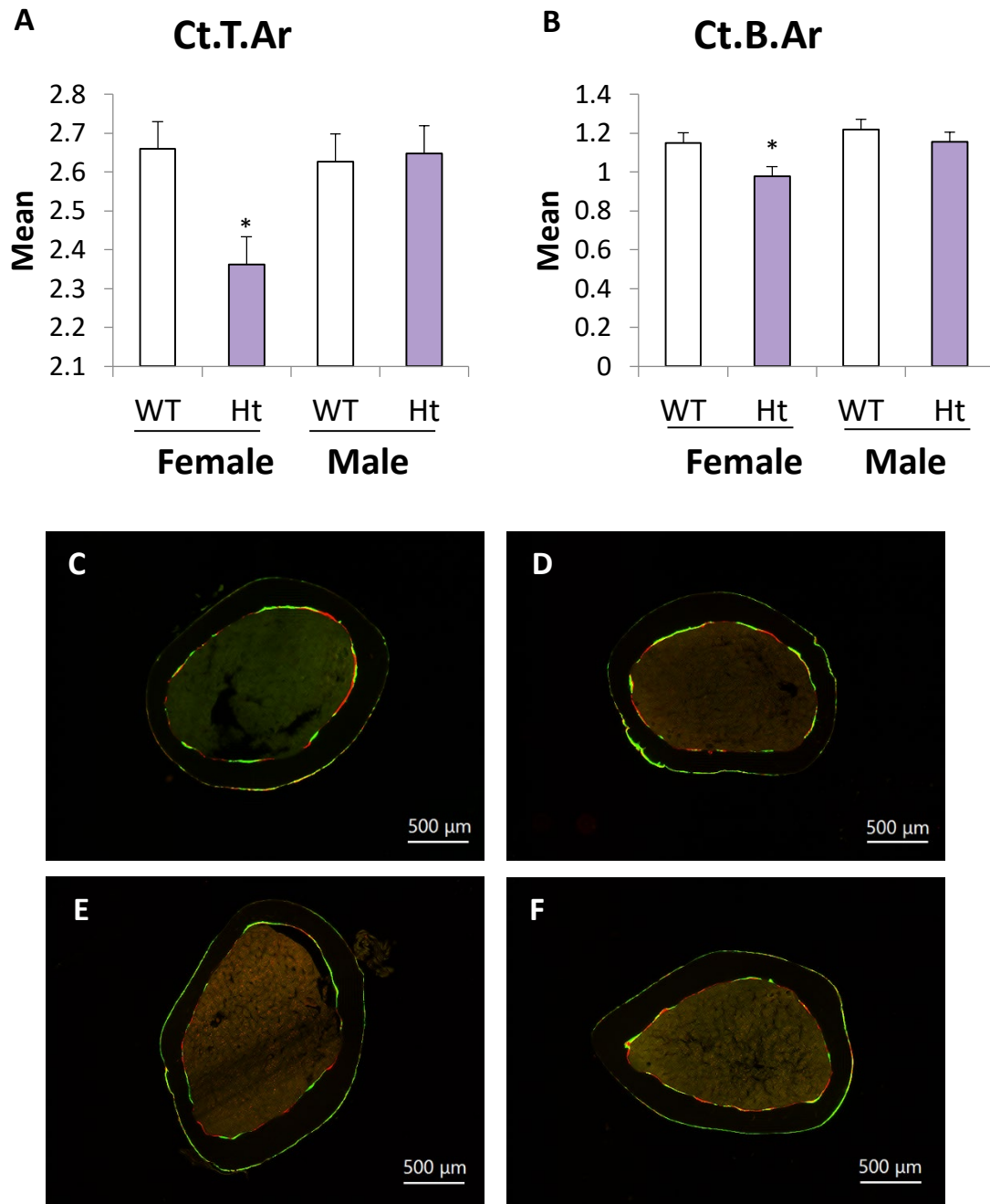
Figure 11. **Female Keap1$^{+/-}$ Mice Have Significantly Smaller Femur Midshafts than WT Females.** Average (A) cortical tissue area and (B) cortical bone area of femur midshaft, accompanied by photos of example (C) wild-type female, (D) Keap1$^{+/-}$ female, (E) Wild-type male, and (F) Keap1$^{+/-}$ male mice. Measurements collected from the femur midshaft of male and female Keap1$^{+/-}$ mice and wild-type controls. Note that *: $p < 0.05$. Bar = 500µm.
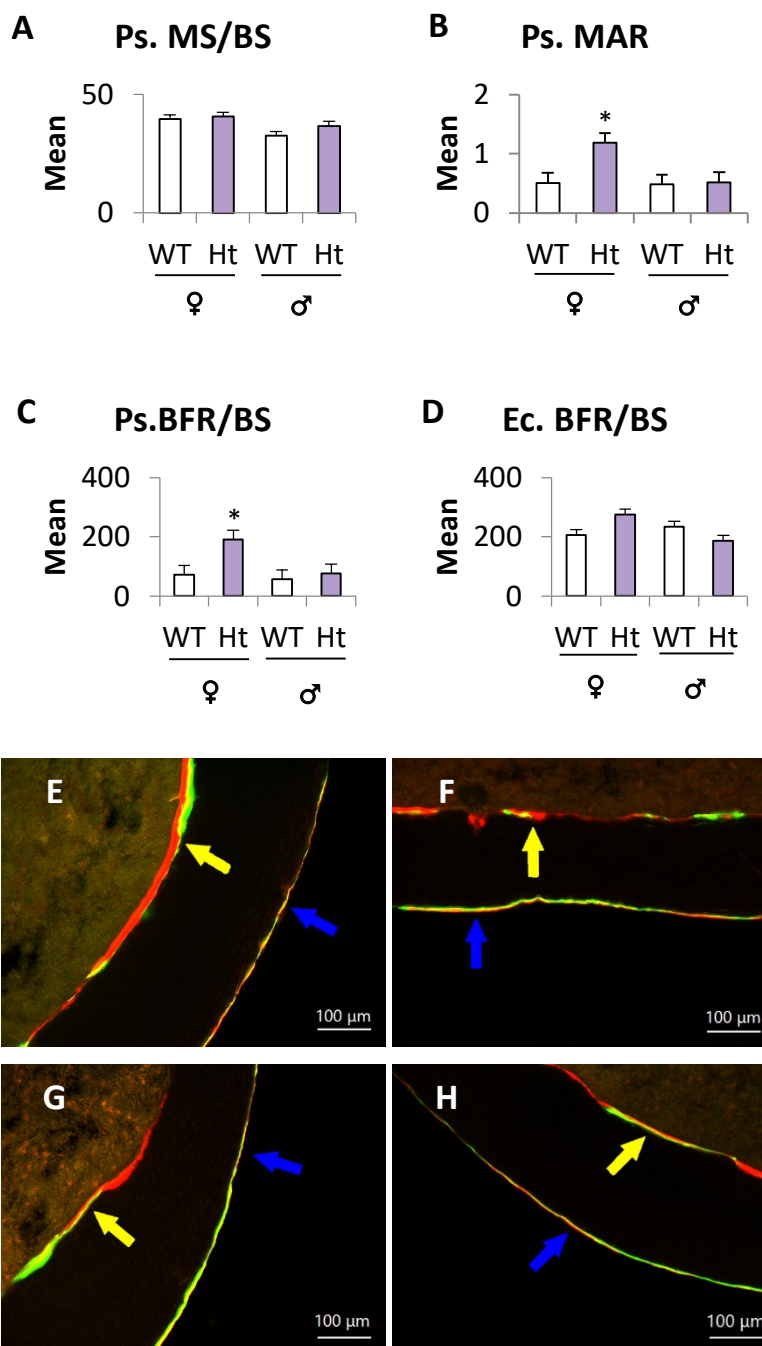
Figure 12. **Dynamic Histomorphometry of Femur Midshaft.** Group averages for (A) periosteal mineralizing surface, (B) periosteal mineral appositional rate, (C) periosteal bone formation rate, and (D) endocortical bone formation rate. Photos illustrate fluorescent labeling of (E) wild-type female, (F) Keap1$^{+/-}$ female, (G) wild-type male, and (H) Keap1$^{+/-}$ male mice. Note that *: $p < 0.05$; Bar = 100μm; blue arrows indicate periosteal surface (Ps); yellow arrows indicate endocortical surface (Ec).

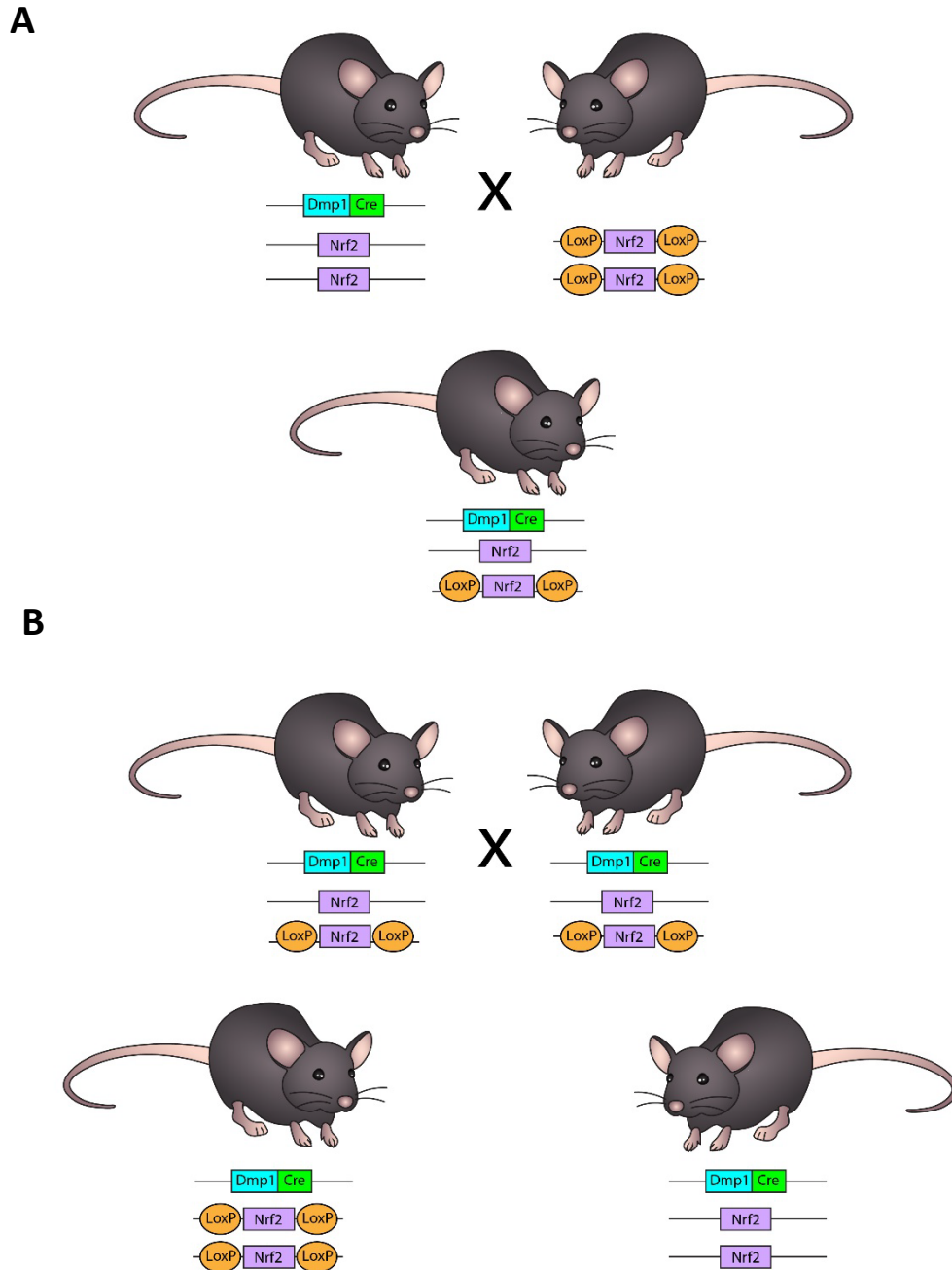**FIGURES: Study 2 – Osteocyte-specific deletion of Nrf2**

Figure 13. **Cre/Lox Breeding Scheme for Generating Dmp1Cre, Nrf2LoxP/LoxP Mice with Wild-Type (Dmp1-Cre, Nrf2+/+) Littermate Controls.** (A) Dmp1-8kb-Cre mice are crossed with Nrf2LoxP/LoxP mice. (B) Hemizygous mice are crossed to generate Dmp1-Cre, Nrf2LoxP/LoxP conditional knockouts and Dmp1-Cre, Nrf2+/+ controls.
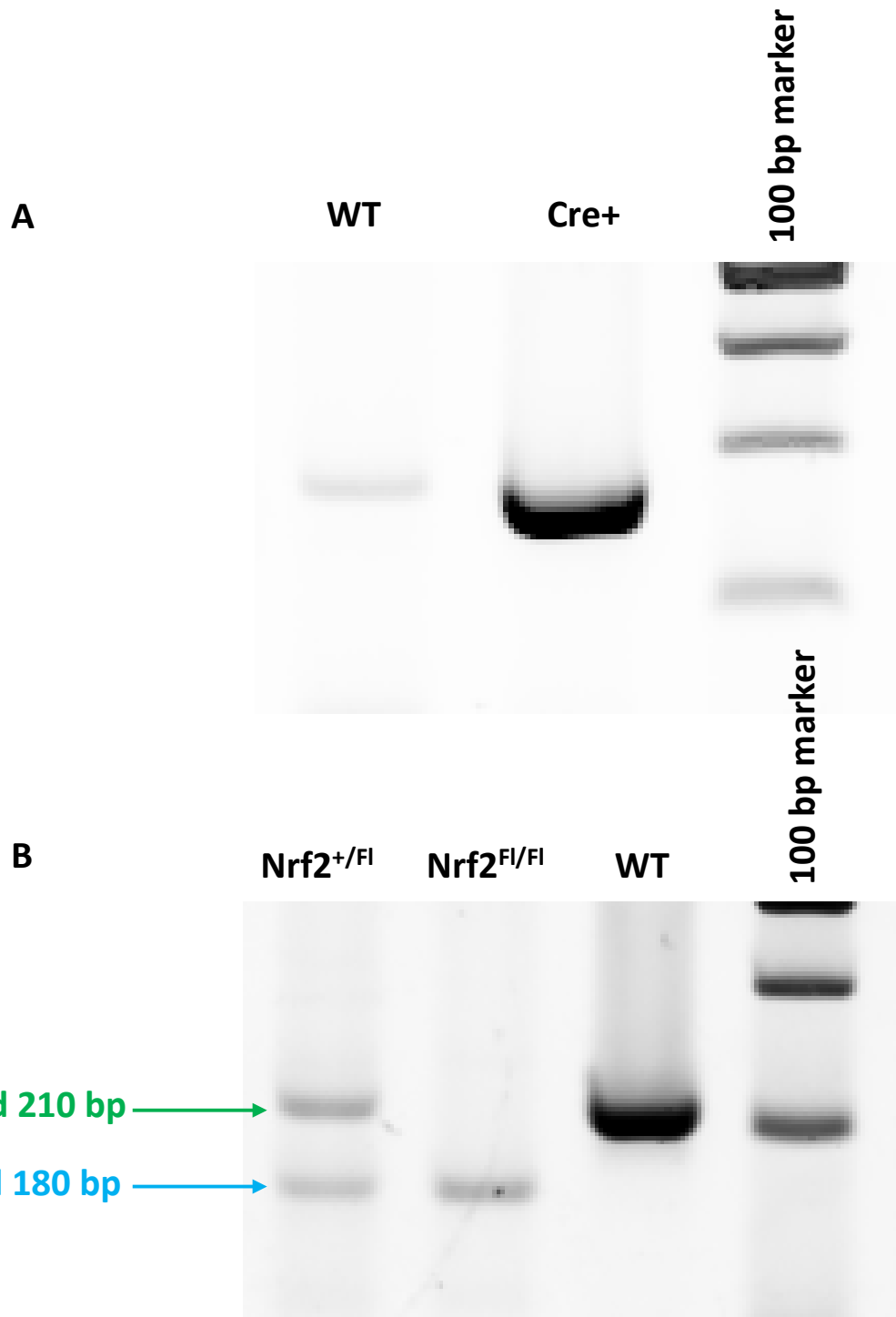
Figure 14. **Dmp1 Cre and Nrf2 LoxP Genotyping.** Electrophoresis gel image displaying amplified bands used to genotype (A) Dmp-Cre and (B) Nrf2 LoxP.
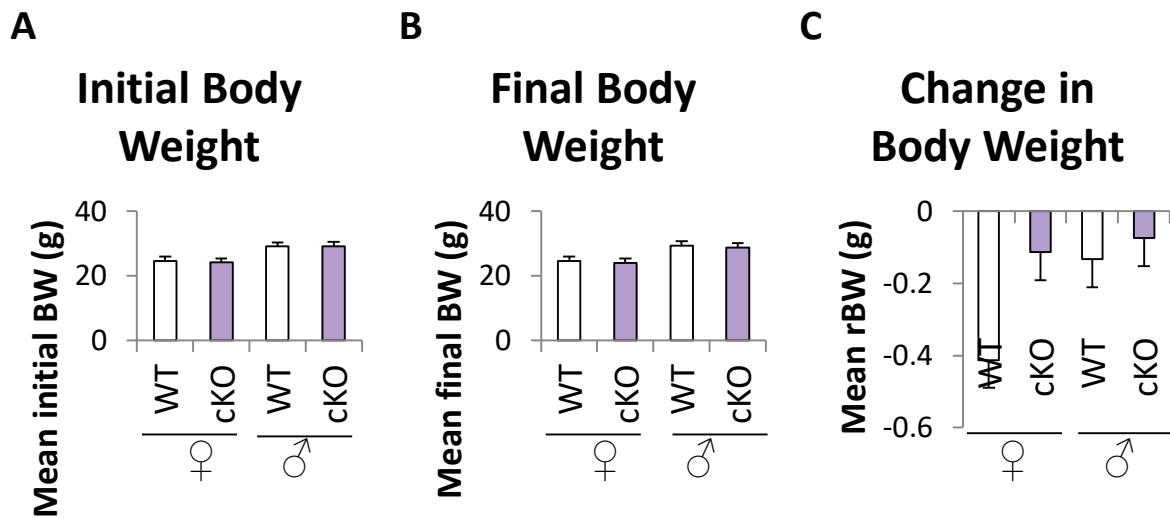
A

Initial Body Weight

B

Final Body Weight

C

Change in Body Weight

Figure 15. **General Characteristics of Dmp1-Cre[+], Nrf2[Flox/Flox] (cKO) Mice.** (A) Initial BW recorded immediately prior to the first round of ulnar loading. (B) Final BW recorded immediately prior to sacrifice. (C) Relative change in BW (rBW) calculated as the difference between final and initial BW.
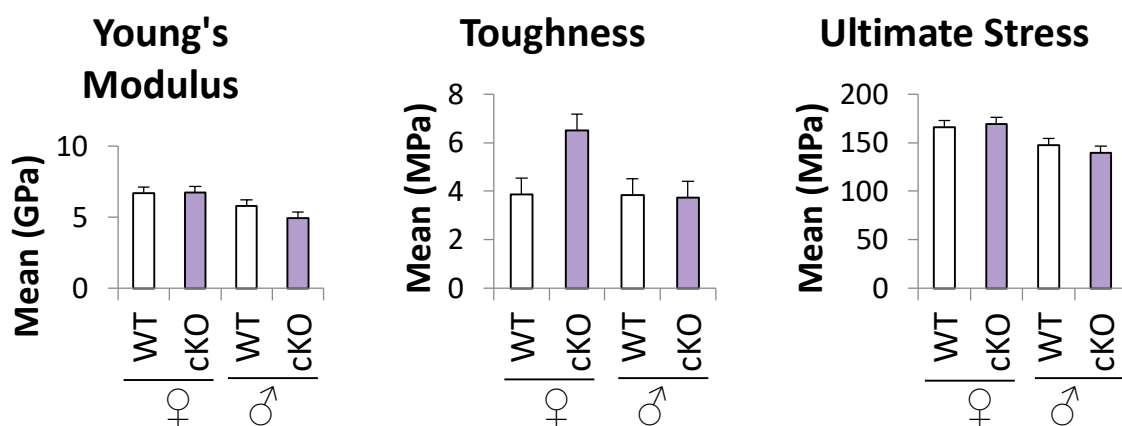
A

Stiffness

Ultimate Force

Total Work

B

Young's Modulus

Toughness

Ultimate Stress
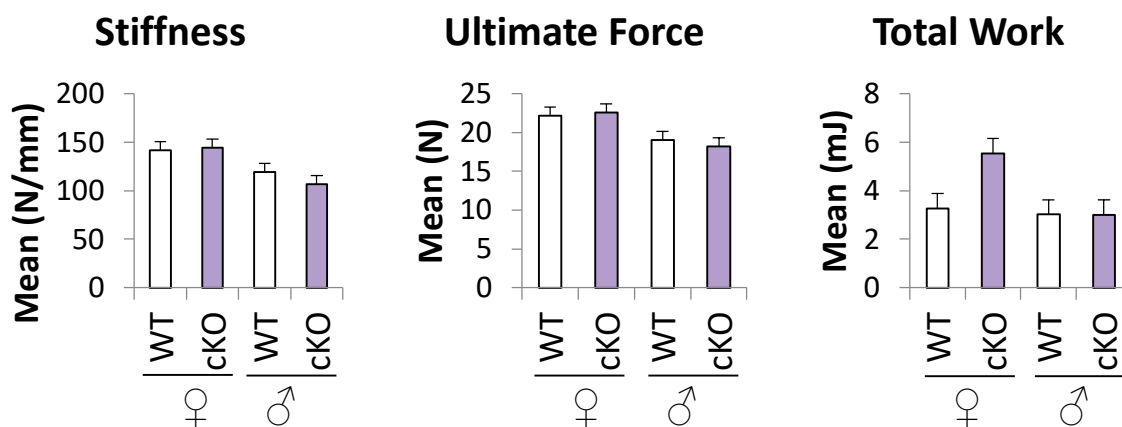
Figure 16. **Biomechanical Property Analysis of Dmp1-Cre$^+$, Nrf2$^{Flox/Flox}$ (cKO) Mice.** (A) Structural properties. Osteocyte-specific deletion of Nrf2 did not affect bone stiffness, ultimate force, or total work. (B) Material properties. Conditional knockout also had no significant effect on Young's Modulus, toughness, or ultimate stress. Data were collected through a 3-point bending test of femora from male and female Dmp1-Cre$^+$, Nrf2$^{Flox/Flox}$ (cKO) mice and wild-type (WT) controls.
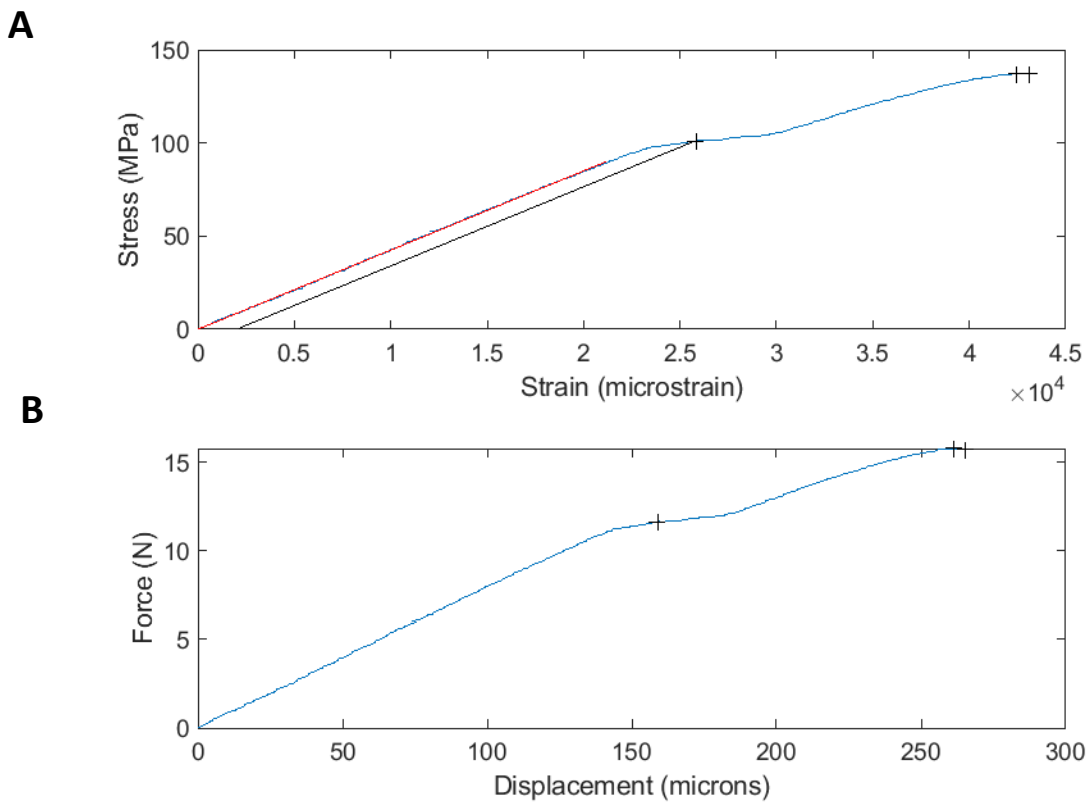
A

B

Figure 17. **3-Point Bending of Dmp1-Cre⁺, Nrf2^{Flox/Flox} (cKO) Mice.** An example (A) Stress/strain curve and (B) force/displacement curve illustrating the 3-point bending test of a Dmp-Cre^{+}, Nrf2$^{Flox/Flox}$ mouse femur.
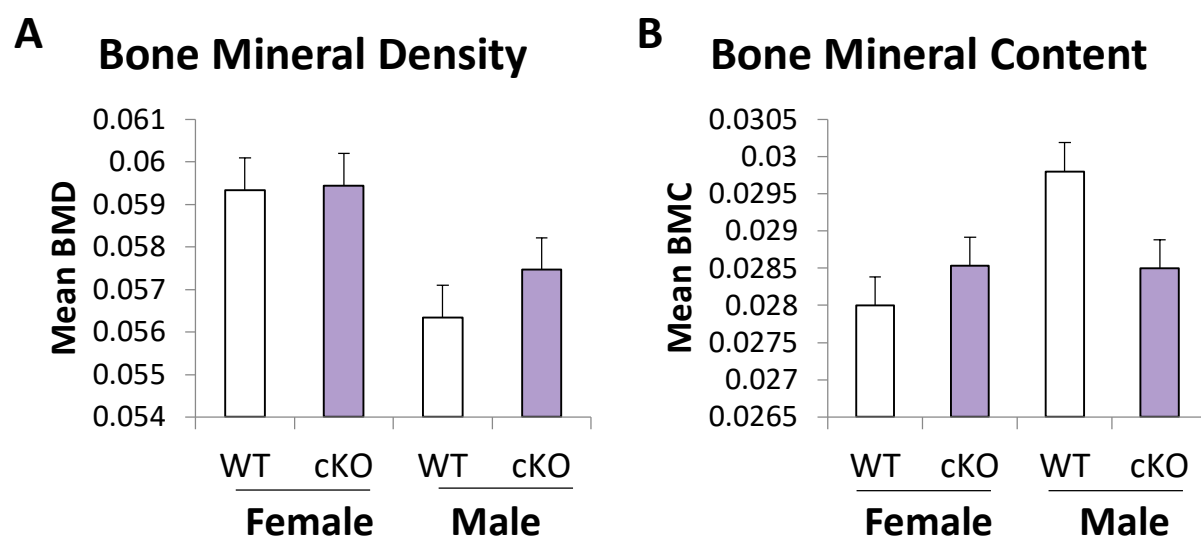
Figure 18. **PIXImus Analysis of Dmp1-Cre+, Nrf2Flox/Flox (cKO) Mice.** No significant differences in either (A) BMD or (B) BMC were observed between cKO animals and their WT controls. Statistical significance was determined using a two-tailed Student's t-test.
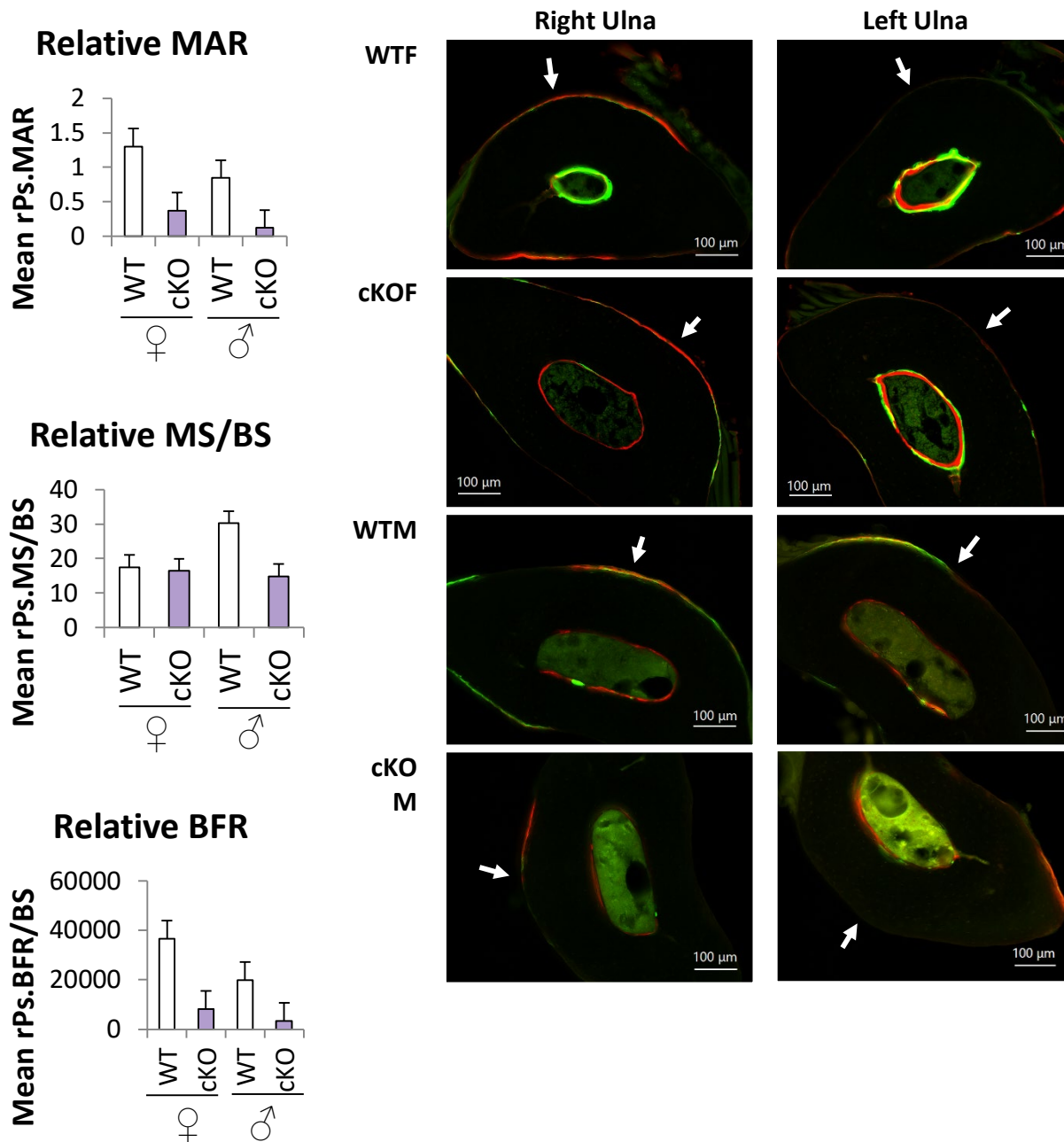
Figure 19. Loading-Induced Bone Formation of Dmp1-Cre$^+$, Nrf2$^{Flox/Flox}$ (cKO) Mice. (A) The relative values, calculated as the difference between the right (loaded) and left (non-loaded) ulnae were calculated to evaluate bone formation activity in the high-strain region of the ulna as a direct result of mechanical loading. (B) Example photos of cortical sections of right and left ulnae from all four test groups. Note that: white arrows indicate the medial surface of the midshaft, where the highest loading strain is applied; bar = 100µm.
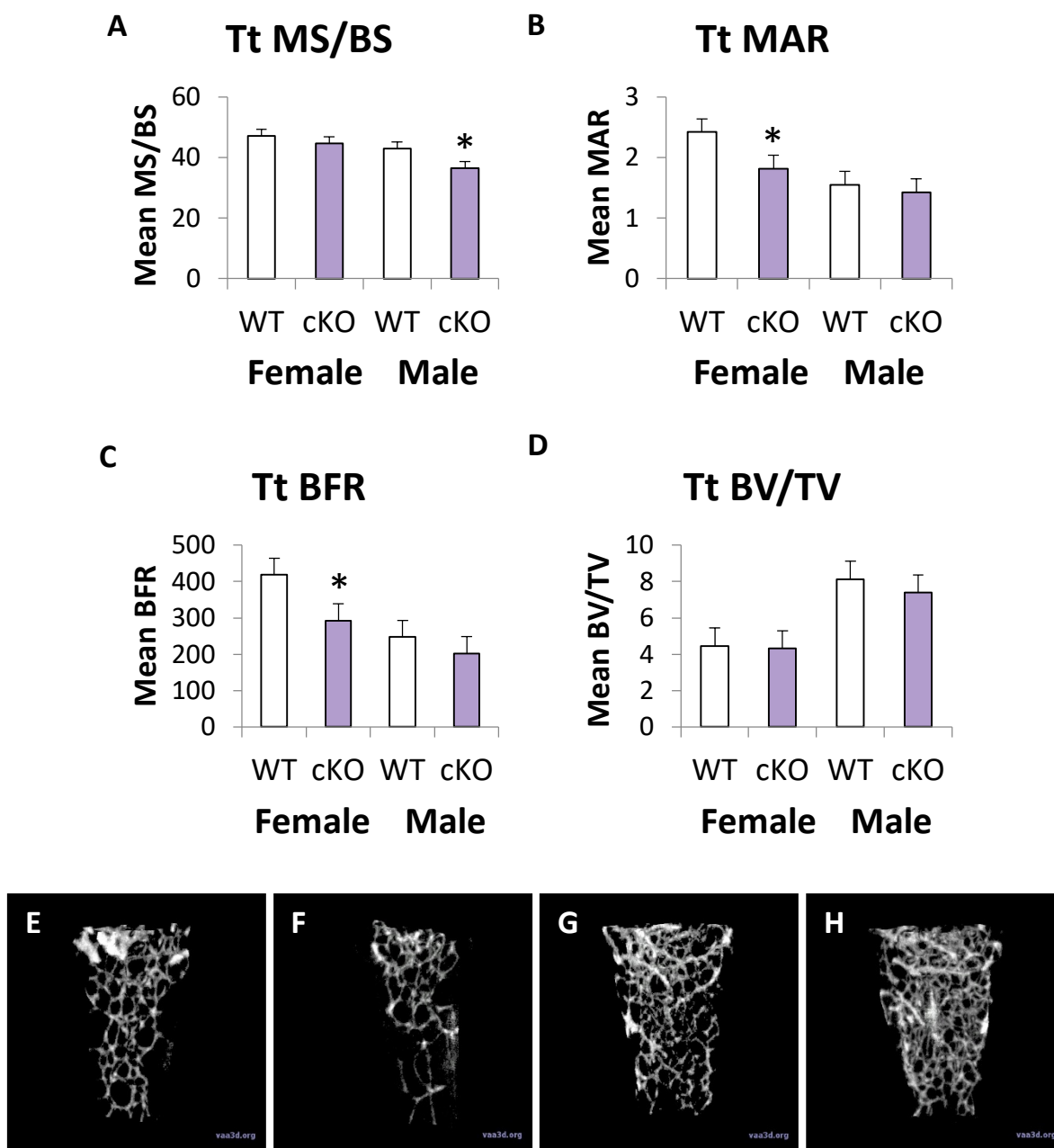
Figure 20. **Results of Dynamic Histomorphometry on Dmp1-Cre[+], Nrf2[Flox/Flox] (cKO) Mice.**
Group averages for (A) mineralizing surface, (B) mineral appositional rate, (C) bone formation
rate, and (D) proportional bone volume. Measurements collected from distal femora of male and
female Dmp1-Cre, Nrf2[Flox/Flox] mice and wild-type controls showed decreased MAR and BFR in
cKO males compared to wild type controls. Statistical significance was determined using a two-
tailed Student's t-test. Note that *: $p < 0.05$.
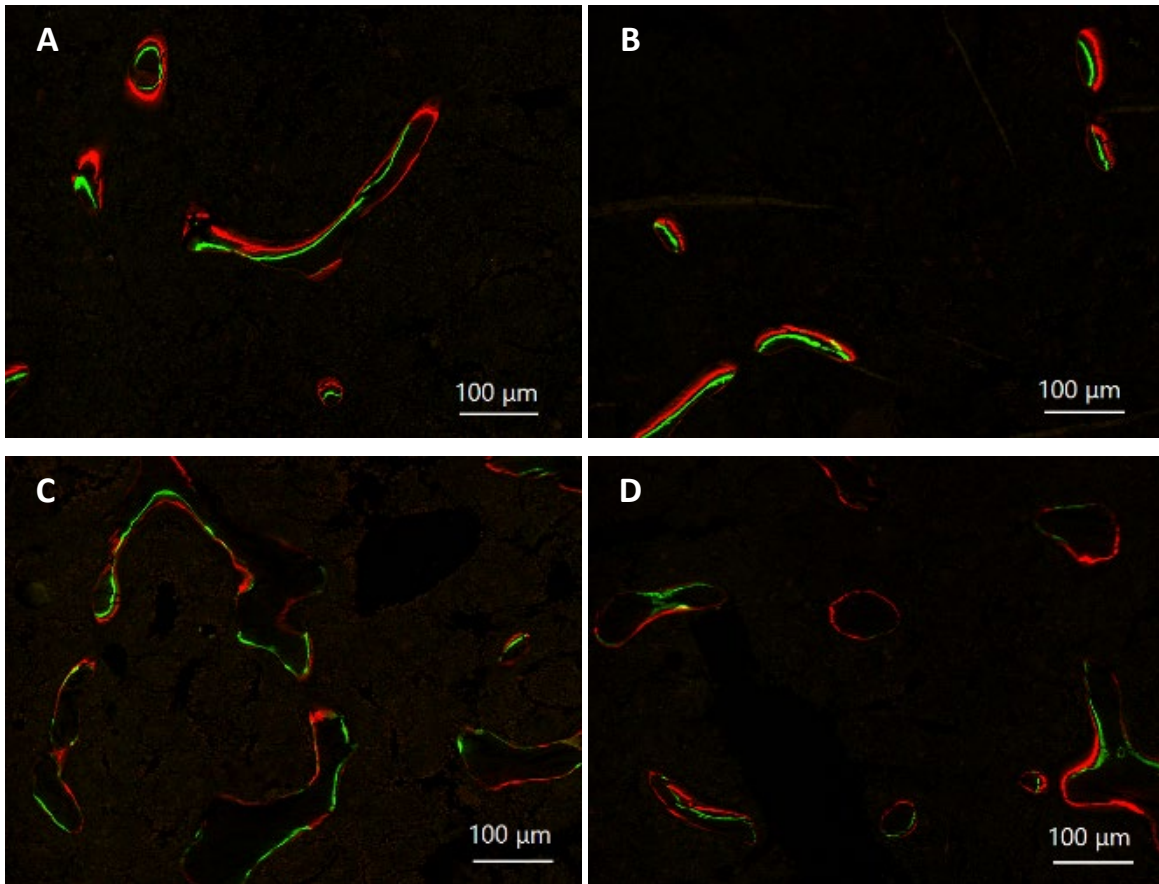
Figure 21. **Fluorescent Labeling of Dmp1-Cre$^+$, Nrf2$^{Flox/Flox}$ (cKO) Mice.** Photos of representative examples of thin section fluorochrome labeling on trabeculae from (A) wild-type female, (B) cKO female, (C) wild-type male, and (D) cKO male mice. Note that bar = 100µm.
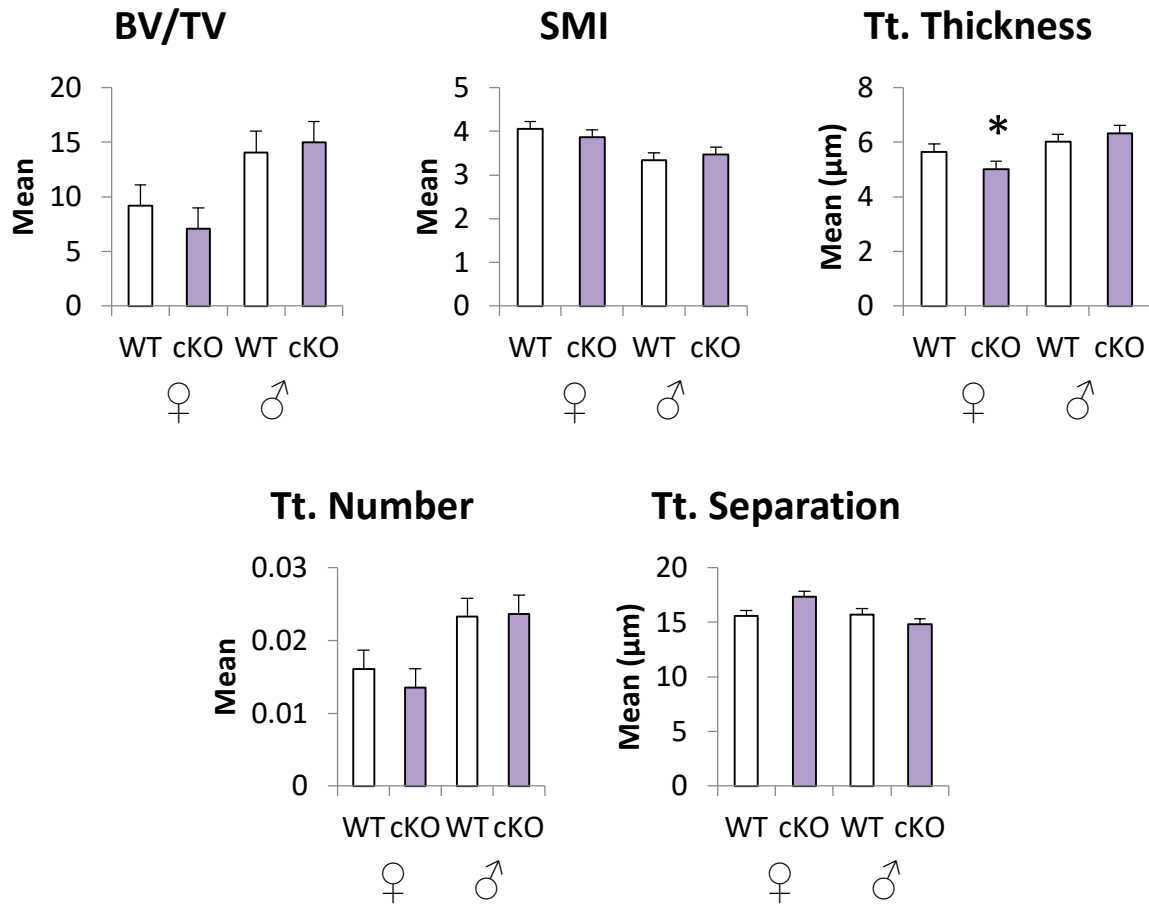
Figure 22. **Trabecular analysis of Dmp1-Cre[+], Nrf2[Flox/Flox] (cKO) Mice.** Results collected from left femora of male and female Dmp1-Cre[+], Nrf2[Flox/Flox] and wild-type controls. Note that *: $p < 0.05$.

FIGURES: Data acquired from previous studies in this lab
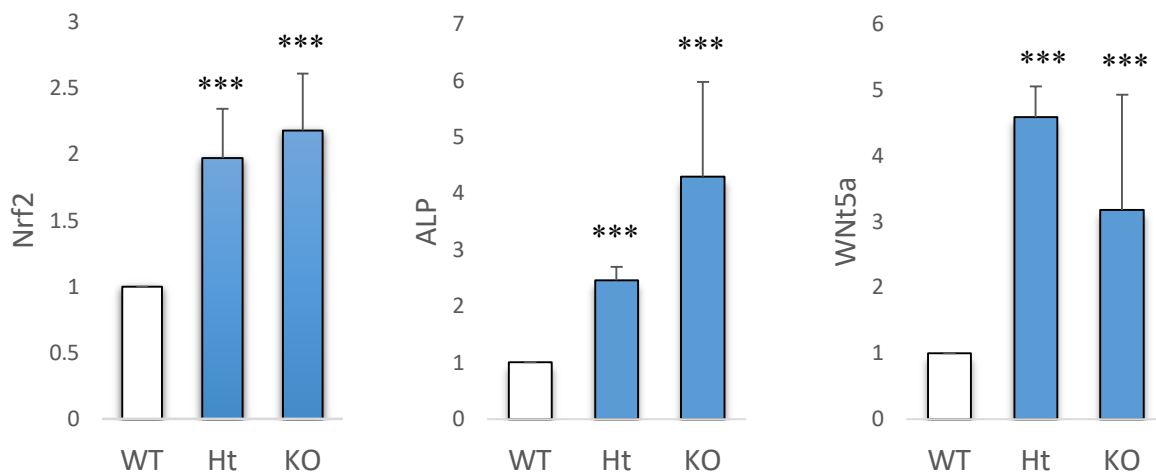
(adapted from Li manuscript in review)

Figure 23. **Nrf2 Activation Follows Keap1 Deletion.** Previous data from this lab acquired via real-time PCR of calvarial osteoblasts from Keap1$^{+/+}$ (WT) Keap1$^{+/-}$ (Ht) and Keap1$^{-/-}$ (KO) mice confirming Keap1$^{+/-}$ animals have moderate activation of Nrf2. Note that: Ht or KO vs. WT, ***: $p < 0.001$.
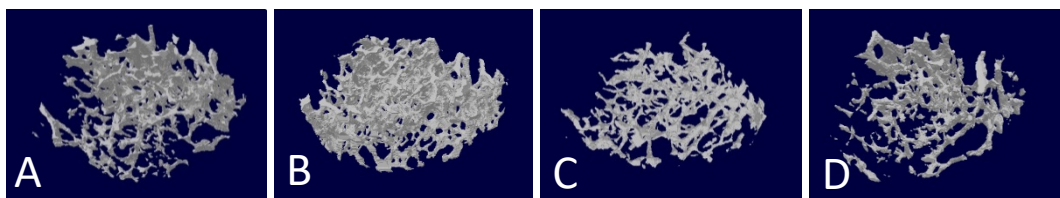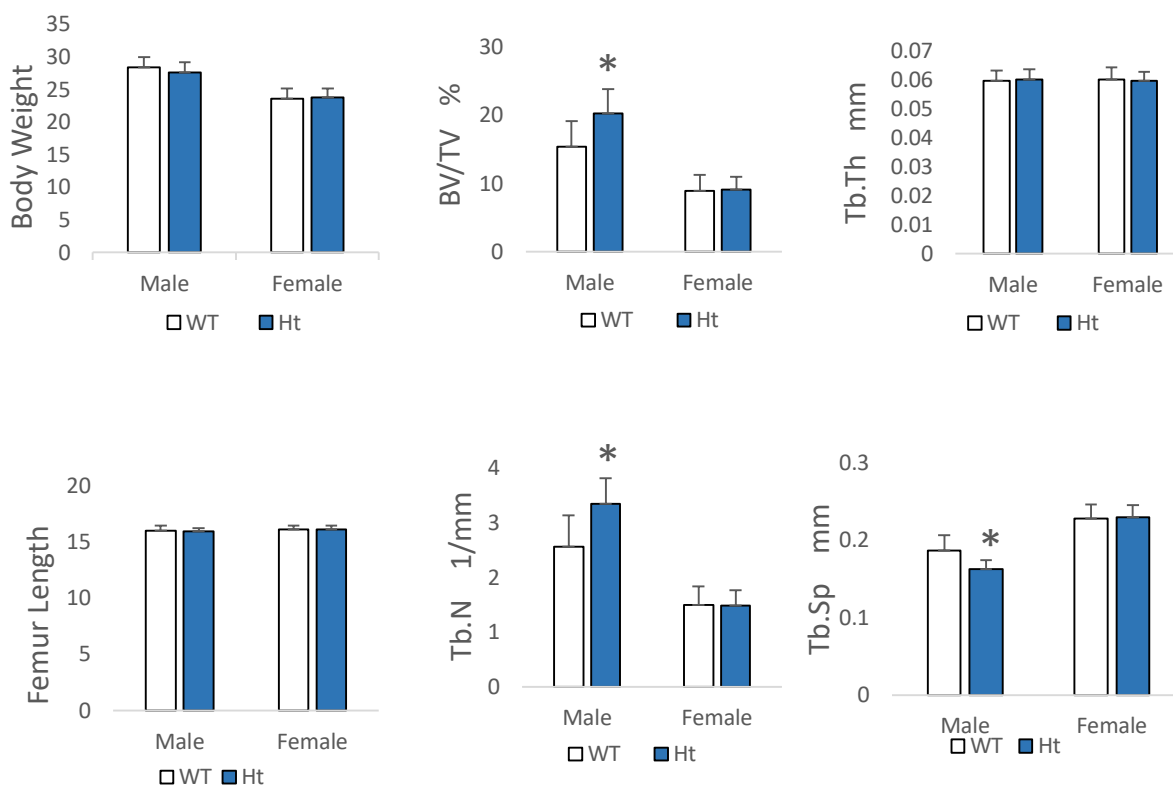
(Adapted from Li manuscript in review)

Figure 24. **Keap1 Heterozygotes have greater Trabecular BV/TV.** Bone volume and structure in Keap1 WT and Ht mice. Results show increased BV/TV, decreased trabecular spacing, and increased trabecular number in Ht males compared to WT males. Accompanying these figures are μ-CT images of distal femur trabecular bone of (A) male WT, (B) male Ht, (C) female WT and (D) female Ht. Note that *: $p < 0.01$ vs. WT.
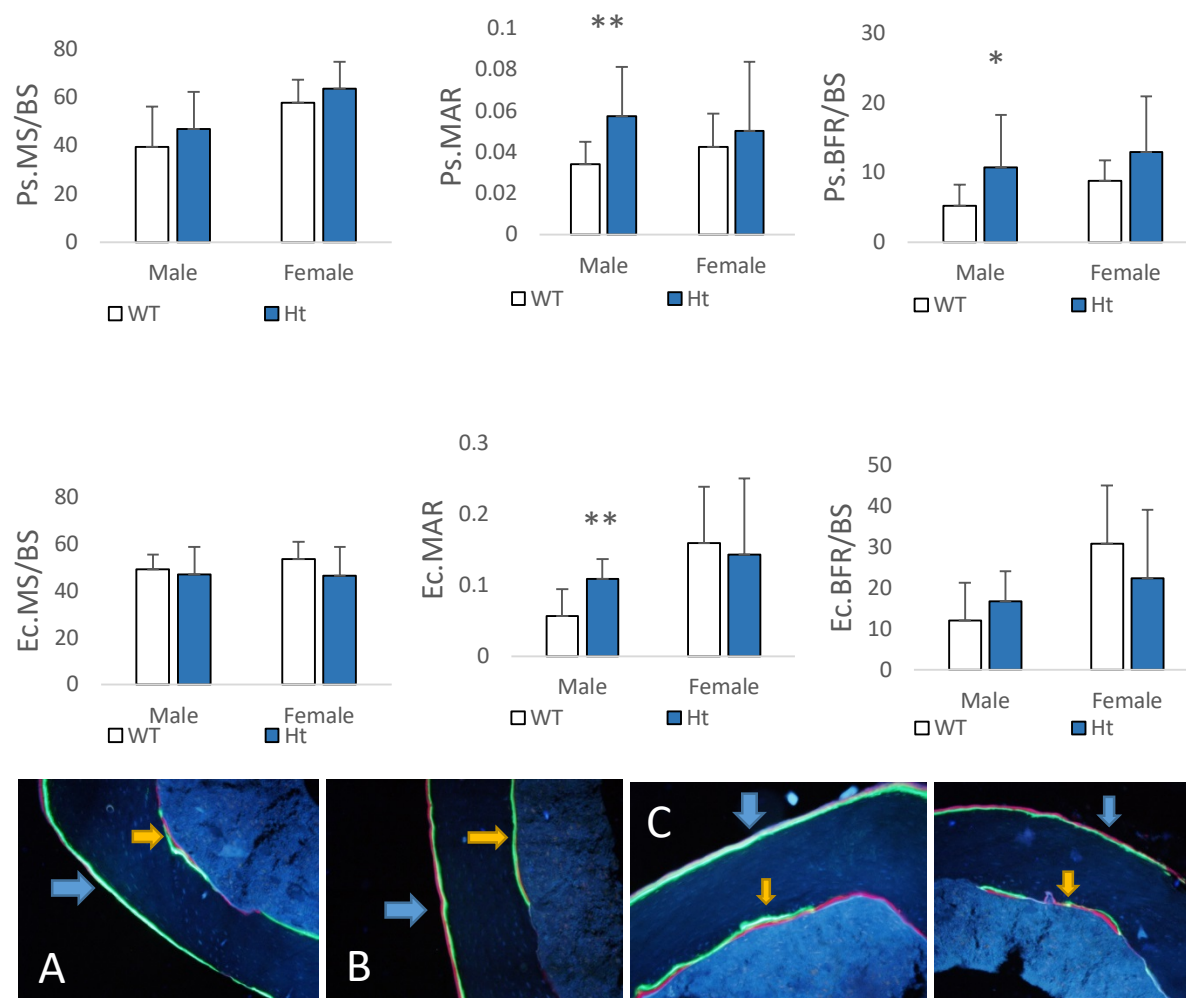
(adapted from Li, manuscript in review)

Figure 25. **Keap1 Heterozygotes Show Increased Loading-Induced Bone Formation.** Dynamic histomorphometry of midshaft femur cortical sections accompanied by photos of the fluorescent labels (calcein and alizarin) in (A) male WT, (B) male Ht, (C) female WT, and (D) female Ht. Cortical bone formation is increased in male Ht mice compared to wild-type controls. Note that *: $p < 0.05$ and **: $p = 0.01$; blue arrows indicate periosteal surface (Ps); yellow arrows indicate endocortical surface (Ec).
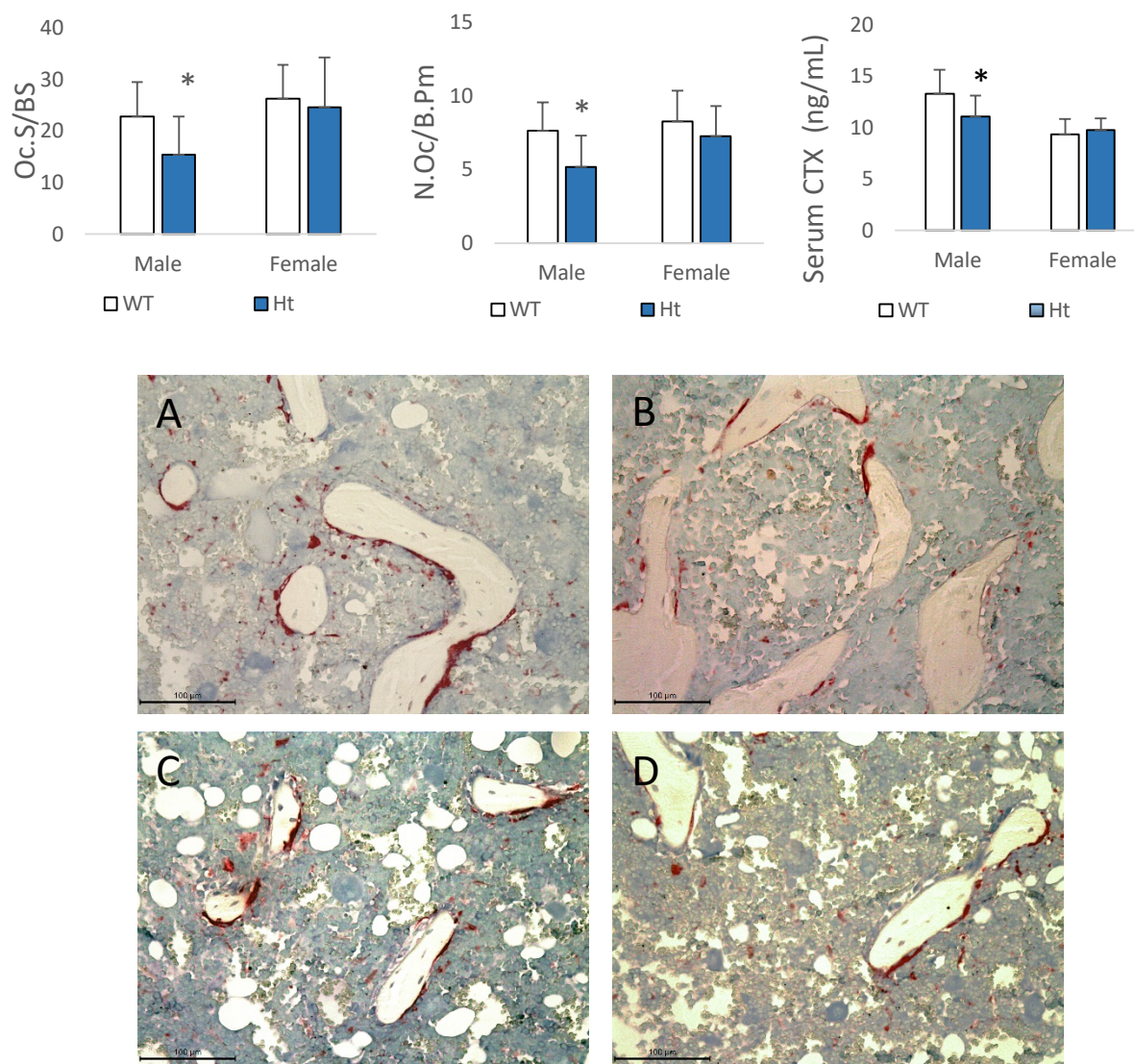
(Adapted from Li, manuscript in review)

Figure 26. **Keap1 Heterozygotes Have Decreased Osteoclast Activity.** TRAP staining analysis of distal femur trabecular bone, accompanied by photos of TRAP stained trabeculae from (A) male WT, (B) male Ht, (C) female WT, and (D) female Ht. Results show significantly decreased osteoclast number, osteoclast surface, and serum CTX in male Ht mice vs. WT controls. Note that *: $p < 0.05$. Bar = 100μm.

REFERENCES

1. Sun, Y.X., et al., *Role of Nrf2 in bone metabolism.* J Biomed Sci, 2015. **22**: p. 101.

2. Seeman, E. and P.D. Delmas, *Bone quality- the material and structural basis of bone strength and fragility.* The New England Journal of Medicine, 2006(21): p. 2250.

3. Ono, T. and T. Nakashima, *Recent advances in osteoclast biology.* Histochemistry & Cell Biology, 2018. **149**(4): p. 325-341.

4. Okamoto, K., et al., *Osteoimmunology: The Conceptual Framework Unifying the Immune and Skeletal Systems.* Physiological Reviews, 2017(4): p. 1295.

5. Sukhodub, L.F. and K.d.p.s.e.u. Dyadyura, *Design and Fabrication of Polymer-Ceramic Nanocomposites Materials for Bone Tissue Engineering.* Проектування та виготовлення полімер-керамічних нанокомпозитних матеріалів для інженерії кісткової тканини, 2018. **10**(6): p. 6003-1-6003-11.

6. Jast, J. and I. Jasiuk, *Age-related changes in the 3D hierarchical structure of rat tibia cortical bone characterized by high-resolution micro-CT.* Journal of Applied Physiology, 2013. **114**(7): p. 923-933.

7. Boyle, W.J., W.S. Simonet, and D.L. Lacey, *Osteoclast differentiation and activation.* Nature, 2003. **423**(6937): p. 337.

8. Pederson, L., et al., *Regulation of Bone Formation by Osteoclasts Involves Wnt/BMP Signaling and the Chemokine Sphingosine-1-Phosphate.* Proceedings of the National Academy of Sciences of the United States of America, 2008. **105**(52): p. 20764.

9. Burr, D.B. and M.R. Allen, *Basic and Applied Bone Biology*, ed. D.B.B.M. Allen. Vol. 1. 2014, 225 Wyman Street, Waltham, MA 02451, USA: Elsevier. 390.

10. Silva, M.J., *Skeletal aging and osteoporosis. [electronic resource] : biomechanics and mechanobiology*. Studies in mechanobiology, tissue engineering and biomaterials: v. 5. 2013: Springer.

11. Burge, R., et al., *Incidence and economic burden of osteoporosis-related fractures in the United States, 2005-2025*. 2007. p. 465-475.

12. Bliuc, D., et al., *Mortality Risk Associated With Low-Trauma Osteoporotic Fracture and Subsequent Fracture in Men and Women.* JAMA, 2009. **301**(5): p. 513-521.

13. Ioannidis, G., et al., *Relation between fractures and mortality: results from the Canadian Multicentre Osteoporosis Study.* CMAJ: Canadian Medical Association Journal = Journal De L'association Medicale Canadienne, 2009. **181**(5): p. 265-271.

14. Zuo, Q., et al., *Characterization of nano-structural and nano-mechanical properties of osteoarthritic subchondral bone.* BMC Musculoskeletal Disorders, 2016. **17**(1): p. 367.

15. Reznikov, N., R. Shahar, and S. Weiner, *Bone hierarchical structure in three dimensions.* Acta Biomaterialia, 2014. **10**(9): p. 3815.

16. Monro, A., *The anatomy of the human bones, nerves, and lacteal sac and duct. [electronic resource] : The ninth edition. By Alexander Monro, Senior, M.D. and F.R.S. fellow of the Royal College of Physicians, and professor of Medicine and Anatomy in the University of Edinburgh.* Eighteenth century collections online. 1777: Printed for J. Balfour. Sold by him and other booksellers there. 420.

17. Chen, F.-M. and X. Liu, *Advancing biomaterials of human origin for tissue engineering.* Progress in polymer science, 2016. **53**: p. 86-168.

18. Leeuwenhoek, A.v., *The select works of Antony Van Leeuwenhoek, containing his microscopical discoveries in many of the works of nature. Translated from the Dutch and Latin editions published by the author, by Samuel Hoole. Part the First.* Vol. 2. 1798, London: printed by Henry Fry, for the translator, and sold by George Nicol, Bookseller to His Majesty, Pall-Mall; J. White, Fleet-Street; J. & A. Arch, Gracechurch Street; and J. Wright, Piccadilly. 396.

19. Havers, C., *Osteologia nova: or, some new observations of the bones, and the parts belonging to them; with the manner of their accretion and nutrition.* 1729, Boston, MA, United States: Francis A. Countway Library of Medicine, Harvard University.

20. Jeong, J.-W., et al., *Protective Effects of Fermented Oyster Extract against RANKL-Induced Osteoclastogenesis through Scavenging ROS Generation in RAW 264.7 Cells.* 2019.

21. Ng, A.Y.H., et al., *Comparative Characterization of Osteoclasts Derived From Murine Bone Marrow Macrophages and RAW 264.7 Cells Using Quantitative Proteomics.* 2018.

22. Arumugam, B., et al., *Characterization of Runx2 phosphorylation sites required for TGF-β1-mediated stimulation of matrix metalloproteinase-13 expression in osteoblastic cells.* Journal Of Cellular Physiology, 2018. **233**(2): p. 1082-1094.

23. Tonna, S. and N.A. Sims, *Talking among ourselves: paracrine control of bone formation within the osteoblast lineage.* Calcified Tissue International, 2014. **94**(1): p. 35-45.

24. Turner, C.H., et al., *Mechanobiology of the Skeleton.* 2009.

25. Ma, W.H., et al., *Neuropeptide Y, substance P, and human bone morphogenetic protein 2 stimulate human osteoblast osteogenic activity by enhancing gap junction intercellular communication.* Brazilian Journal of Medical and Biological Research, 2015(4): p. 299.

26. Robling, A.G., A.B. Castillo, and C.H. Turner, *BIOMECHANICAL AND MOLECULAR REGULATION OF BONE REMODELING.* Annual Review of Biomedical Engineering, 2006. **8**(1): p. 455-498.

27. Wang, M., et al., *Periosteal PTHrP regulates cortical bone modeling during linear growth in mice.* 2014. p. 71-82.

28. Hsieh, H.-J., et al., *Shear-induced endothelial mechanotransduction: the interplay between reactive oxygen species (ROS) and nitric oxide (NO) and the pathophysiological implications.* Journal of Biomedical Science, 2014. **21**(1): p. 1-33.

29. Zhou, T., et al., *Endothelial Mechanotransduction Mechanisms for Vascular Physiology and Atherosclerosis.* Journal of Mechanics in Medicine & Biology, 2014. **14**(5): p. -1.

30. Tschumperlin, D.J., *Mechanotransduction.* Comprehensive Physiology, 2011. **1**(2): p. 1057-1073.

31. Torrance, A.G., et al., *Noninvasive loading of the rat ulna in vivo induces a strain-related modeling response uncomplicated by trauma or periostal pressure.* Calcified Tissue International, 1994. **54**(3): p. 241-247.

32. Li, J., et al., *The P2X7 Nucleotide Receptor Mediates Skeletal Mechanotransduction.* Journal of Biological Chemistry, 2005. **280**(52): p. 42952-42959.

33. Itoh, K., J. Mimura, and M. Yamamoto, *Discovery of the Negative Regulator of Nrf2, Keap1: A Historical Overview.* Antioxidants & Redox Signaling, 2010. **13**(11): p. 1665-1678.

34. Pagano, G., *Redox-modulated xenobiotic action and ROS formation: a mirror or a window?* Human & Experimental Toxicology, 2002. **21**(2): p. 77-81.

35. Bardaweel, S.K., et al., *Reactive Oxygen Species: the Dual Role in Physiological and Pathological Conditions of the Human Body.* The Eurasian Journal of Medicine, 2018(3): p. 193.

36. Yen, C.-H. and H.-H. Hsiao, *NRF2 Is One of the Players Involved in Bone Marrow Mediated Drug Resistance in Multiple Myeloma.* International Journal Of Molecular Sciences, 2018. **19**(11).

37. Manchester, L.C., et al., *Melatonin: an ancient molecule that makes oxygen metabolically tolerable.* J Pineal Res, 2015. **59**(4): p. 403-19.

38. Thimmulappa, R.K., et al., *Preclinical evaluation of targeting the Nrf2 pathway by triterpenoids (CDDO-Im and CDDO-Me) for protection from LPS-induced inflammatory response and reactive oxygen species in human peripheral blood mononuclear cells and neutrophils.* Antioxidants and Redox Signaling, 2007. **9**(11): p. 1963-1970.

39. Huang, Y., et al., *The complexity of the Nrf2 pathway: beyond the antioxidant response.* J Nutr Biochem, 2015. **26**(12): p. 1401-13.

40. Ichimura, Y., et al., *Phosphorylation of p62 Activates the Keap1-Nrf2 Pathway during Selective Autophagy.* Molecular Cell, 2013. **51**(5): p. 618-631.

41. Moi, P., et al., *Isolation of NF-E2-related factor 2 (Nrf2), a NF-E2-like basic leucine zipper transcriptional activator that binds to the tandem NF-E2/AP1 repeat of the beta-globin locus control region.* 1994.

42. Sun, Y.X., et al., *Deletion of Nrf2 reduces skeletal mechanical properties and decreases load-driven bone formation.* Bone, 2015. **74**: p. 1-9.

43. Kloska, D., et al., *Nrf2 Sequesters Keap1 Preventing Podosome Disassembly: A Quintessential Duet Moonlights in Endothelium.* Antioxidants & Redox Signaling, 2019. **30**(14): p. 1709-1730.

44. Chen, Q.M. and A.J. Maltagliati, *Nrf2 at the Heart of Oxidative Stress and Cardiac Protection.* Physiol Genomics, 2017: p. physiolgenomics.00041.2017.

45. Beyer, T.A., et al., *Impaired liver regeneration in Nrf2 knockout mice: role of ROS-mediated insulin/IGF-1 resistance.* Embo j, 2008. **27**(1): p. 212-23.

46. Zenkov, N.K., et al., *Mazes of Nrf2 regulation.* Biochemistry (Moscow), 2017(5): p. 556.

47. Bresciani, A., et al., *Nuclear factor (erythroid-derived 2)-like 2 (NRF2) drug discovery: Biochemical toolbox to develop NRF2 activators by reversible binding of Kelch-like ECH-associated protein 1 (KEAP1).* Archives Of Biochemistry And Biophysics, 2017. **631**: p. 31-41.

48. Ajiboye, T.O., M.T. Yakubu, and A.T. Oladiji, *Electrophilic and Reactive Oxygen Species Detoxification Potentials of Chalcone Dimers is Mediated by Redox Transcription Factor Nrf-2.* Journal of Biochemical and Molecular Toxicology, 2014(1): p. 11.

49. Katsumata, Y., et al., *Single Local Injection of Epigallocatechin Gallate-Modified Gelatin Attenuates Bone Resorption and Orthodontic Tooth Movement in Mice*. 2018.

50. Liu, S., et al., *Gastrodin protects MC3T3-E1 osteoblasts from dexamethasone-induced cellular dysfunction and promotes bone formation via induction of the NRF2 signaling pathway.* 2018.

51. Sakai, E., et al., *Effects of deficiency of Kelch-like ECH-associated protein 1 on skeletal organization: A mechanism for diminished nuclear factor of activated T cells cytoplasmic 1 during osteoclastogenesis.* FASEB Journal, 2017. **31**(9): p. 4011-4022.

52. Yoshida, E., et al., *Hyperactivation of Nrf2 leads to hypoplasia of bone in vivo.* Genes to Cells, 2018(5): p. 386.

53. Bivi, N., et al., *Cell autonomous requirement of connexin 43 for osteocyte survival: consequences for endocortical resorption and periosteal bone formation.* 2012.

54. Xue, P., et al., *Adipose Deficiency of Nrf2 in ob/ob Mice Results in Severe Metabolic Syndrome.* 2013.

55. Blazek, J.D., et al., *Disruption of bone development and homeostasis by trisomy in Ts65Dn Down syndrome mice.* 2010.

56. Moore, D.S. and G.P. McCabe, *Introduction to the practice of statistics*. 1989: W.H. Freeman. 790.